



INSTITUT DE FRANCE
Académie des sciences

Comptes Rendus

Géoscience

Sciences de la Planète

Govind Oinam, A. Krishnakanta Singh, Mallickarjun Joshi, Amrita Dutt, M. Rajanikanta Singh, N. Lakhan Singh and R. K. Bikramaditya Singh


Continental extension of northern Gondwana margin in the Eastern Himalaya: Constraints from geochemistry and U–Pb zircon ages of mafic intrusives in the Siang window, Arunachal Himalaya, India

Volume 352, issue 1 (2020), p. 19-41.

<https://doi.org/10.5802/crgeos.6>

© Académie des sciences, Paris and the authors, 2020.

Some rights reserved.

 This article is licensed under the
CREATIVE COMMONS ATTRIBUTION 4.0 INTERNATIONAL LICENSE.
<http://creativecommons.org/licenses/by/4.0/>



*Les Comptes Rendus. Géoscience — Sciences de la Planète sont membres du
Centre Mersenne pour l'édition scientifique ouverte*

www.centre-mersenne.org



Petrology, Geochemistry — Original Article

Continental extension of northern Gondwana margin in the Eastern Himalaya: Constraints from geochemistry and U–Pb zircon ages of mafic intrusives in the Siang window, Arunachal Himalaya, India

Govind Oinam^a, A. Krishnakanta Singh^{*,a}, Mallickarjun Joshi^b, Amrita Dutt^a,
M. Rajanikanta Singh^a, N. Lakhan Singh^a and R. K. Bikramaditya Singh^b

^a Wadia Institute of Himalayan Geology, GMS Road, Dehradun - 248001, India

^b Department of Geology, Banaras Hindu University, Varanasi - 221005, India.

E-mails: govindoinam@gmail.com (G. Oinam), aksingh_wihg@rediffmail.com (A. K. Singh), mallickbhu@gmail.com (M. Joshi), amritadutt6@gmail.com (A. Dutt), rajanimutum@gmail.com (M. R. Singh), neesam10@gmail.com (N. L. Singh), rkaditya17@rediffmail.com (R. K. B. Singh).

Abstract. We report new U–Pb zircon age and whole-rock geochemical data from the Pangin mafic intrusive rocks of the Siang window, eastern Himalayas. These mafic rocks are medium to coarse-grained gabbros, consisting mainly of plagioclase and clinopyroxene with accessory phases (hornblende + Fe–Ti oxides) that retain granular and interlocking texture. Geochemically, they display enriched-mid oceanic ridge basalt (E-MORB) affinity characterized by moderate to slightly fractionated REE patterns marked by $(La/Yb)_N = 2.65 - 3.99$. Their geochemical characteristics suggest that the parental magmas of these rocks were formed by medium to higher degrees (~12–28%) of partial melting similar to that of the asthenospheric mantle in the garnet-spinel transition zone. Magmatic zircons from two gabbros yield U–Pb ages of 521.50 ± 2.53 Ma and 568 ± 2 Ma. This new age reveals two pulses of Late Neoproterozoic and Early Cambrian mafic magmatism that are inconsistent with the temporal distribution of Paleozoic magmatism in the Siang window of the Eastern Himalayas. However, based on the results of this study and the correlation of continental extensional mafic magmatism in the Northwest Himalaya, we suggest that investigated mafic intrusive rocks might have been generated in an extensional tectonic environment during the long-lasting Pan-African orogenic cycle of the late Neoproterozoic to early Cambrian which ended with the formation of the Gondwana supercontinent.

Keywords. Zircon U–Pb, Mafic intrusives, Siang window, Eastern Himalayas, Pan-African orogeny.

Manuscript received 21st December 2019, revised 1st March 2020 and 8th March 2020, accepted 9th March 2020.

* Corresponding author.

1. Introduction

The late Neoproterozoic to early Cambrian was an important time interval in the geological evolution of the Gondwana supercontinent because it was the period of assembly of this supercontinent as well as subduction initiation in the Peri-Gondwana margin [Cawood and Buchan, 2007, Cawood *et al.*, 2007, Collins and Pisarevsky, 2005, Li *et al.*, 2008a,b, Meert, 2003, Murphy *et al.*, 2011]. It is also proposed that the eastern Gondwana assembly took place during 570–510 Ma, and subduction initiation in the Gondwana proto-Pacific margin happened during 580–550 Ma [Cawood and Buchan, 2007, Meert, 2003]. Subduction of the proto-Tethyan oceanic lithosphere during Late Neoproterozoic to Early Cambrian along the northern margin of Gondwana was responsible for the arc magmatism which occurred along the northern part of the Gondwana supercontinent [Nadimi, 2007, Ramezani and Tucker, 2003, Ustaömer *et al.*, 2009]. The Indian proto-Tethyan margin witnessed the formation of extensively distributed Early Paleozoic granitoids thought to be emplaced during the final assembly of Gondwana [Baig *et al.*, 1988, Gaetani and Garzanti, 1991, Meert and Van Der Voo, 1997]. Cawood *et al.* [2007] proposed the possible existence of the “North India Orogen” in the Early Cambrian (530–490 Ma) and interpreted the granitoids as a result of an Andean-type magmatism due to the southward subduction of the proto-Tethyan lithosphere below the Indian plate. Continued southward subduction of proto-Tethyan lithosphere produced gravitational sinking which led to slab roll-back resulting in asthenospheric upwelling and back-arc extension along the northern margin of Gondwana [Gürsu *et al.*, 2015, Zhu *et al.*, 2012]. This type of magmatism was reported from the Australian proto-Tethyan margin (Kalkarindji basalts, in North-east Australia), south-western part of Turkey [Gürsu and Göncüoğlu, 2005] and northern Arabian plate [Gürsu *et al.*, 2015]. Gaetani and Garzanti [1991] argued that the Early Paleozoic granitoids might have been associated with the formation of the Gondwana supercontinent while others (e.g. Hughes and Jell, 1999, Murphy and Nance, 1991) questioned the supercontinent breakup. Concerning the evolution of the early Paleozoic granitoids, either the late Pan-African orogeny [Islam *et al.*, 1999, Valdiya, 1995] or mantle involvement, due to the presence of dark mi-

cro granular enclaves [Le Fort *et al.*, 1986, Miller *et al.*, 2001] are proposed. The knowledge of the processes responsible for these intrusions is important for the evolution of the pre-collision margin of northern India, but it still remains controversial.

The Himalayan Mountain Belt has experienced several phases of mafic magmatism ranging in age from late Precambrian to Cenozoic periods [Bhat, 1987]. These magmatic activities can be found as volcanic flows and mafic dykes throughout the belt. The Precambrian mafic magmatic rocks are best exposed in western Himalaya and are well studied compared to their eastern counterparts [Ahmad and Bhat, 1987, Ahmad and Tarney, 1991, Ahmad *et al.*, 1999, Srivastava and Sahai, 2001]. Geochemical characteristics imply that these magmas were derived from an enriched lithospheric mantle source in an extensional tectonic setting with variable degrees of partial melting [Ahmad, 2008].

In the eastern Himalaya, geological and geochemical investigations have been conducted on the Abor mafic volcanic rocks of the Siang Window [Acharyya, 1994, Ali *et al.*, 2012, Bhat, 1984, Bhat and Ahmad, 1990, Jain and Thakur, 1978, Kumar, 1997, Liebke *et al.*, 2011, Sengupta *et al.*, 1996, Singh, 1993, 2006, 2007, Singh and Singh, 2012, Singh *et al.*, 2019], and the associated felsic volcanics [Singh and Singh, 2012, Singh *et al.*, 2019, Talukdar and Majumdar, 1983]. However, the age and geochemical evolution of the mafic intrusives have not been studied in detail despite their importance in understanding the nature of magmatism and the formation of new crust at the eastern tip of the Indian sub-continent. Also, their petrogenetic relationship with the mafic and felsic rocks of Abor Volcanics is still unknown. One of such intrusions occurs in the western part of the Siang window where it is exposed in association with carbonates of the Buxa formation. This mafic intrusion is interpreted to have been formed in an extensional setting, and a late Neoproterozoic age has been assigned on the basis of microfossils – *Rivularia haematites* and *Filamentous cyanobacteria* – present in the dolomites of the Buxa formation [Singh and Tewari, 2010]. In this paper, we present for the first time U-Pb zircon ages and new whole-rock geochemical data of the mafic intrusions from the Pangin area of the Siang window, eastern Himalaya in order to understand their petrogenesis and emplacement mechanism.

2. Geological background

The Himalayan mountain range of India is geographically classified into (i) Siwaliks which occupy the footwall of Main Boundary Thrust (MBT), (ii) Lesser Himalaya bounded by MBT in the south and Main Central Thrust (MCT) in the north and (iii) Higher Himalaya between MCT and South Tibetan Detachment (STD) (Figure 1; Hodges *et al.* [2000] and Yin [2006]). The eastern Himalaya is a ~350 km long fold-thrust belt which extends from the eastern part of Bhutan up to the Dibang and Lohit valleys of Arunachal Pradesh. The Siang valley is a part of the eastern Himalaya and major litho-tectonic units show a bend in their regional strike from NE-SW in the west to NW-SE in the east throughout the Siang gorge. This unit is known as the Eastern Syntaxial Bend (Figure 1b; Wadia [1931]). The folded core structure of this syntaxis is also known as the Siang antiform [Singh, 1993] and the Siang window [Acharyya, 1998]. Acharyya [1998] suggested that the Siang window evolved during the southern exhumation of the Higher Himalayan Crystalline Complex and the southward thrusting of the Tertiary Himalayan foreland basin.

The lithological association of the Siang window comprises the Miri-Buxa Groups of meta-sedimentary interbedded rocks that are folded with the Abor volcanics and Yinkiong sedimentary formations (Figure 1b). The lithological units inside the window are dissected by numerous normal faults that are oblique to both North Pasighat Thrust (NPT) in the southern part and MBT in the northern part of the window [Acharyya, 2007, Kumar, 1997]. These faults control the duplex geometry and the antiform nature of the Siang window [Acharyya and Sengupta, 1998] (Figure 1c). Acharyya [2007] reported NPT as the southern continuity of MBT and another arm in the window's roof. The Abor volcanics which occupy the core of the Siang window are grouped into (i) mafic volcanics which are found as lava flows and include basalt, agglomeratic basalts, sills, dykes with minor amount of tuffs, volcanic breccias, lapilli and pillow basalt; (ii) felsic volcanics such as rhyolite, dacite and welded tuff; and (iii) mafic intrusives including gabbro and diorite. The Buxa formation in the western part of the window consists of quartzite, dolomite, mafic intrusives and fossiliferous carbonates [Kumar, 1997, Singh, 1993, 1999]. This formation

is surrounded by the Higher Himalaya and further succeeded by the Yang-sang-chu formation in the north [Singh, 1993]. The Abor Volcanics are underlain by the Miri Quartzite which is mainly white, purple and pink-coloured mature quartzite. The Miri quartzites have also been intruded by mafic rocks near its boundary with the volcanics (Figure 1b) [Acharyya, 2007]. The Yinkiong Formation overlying the Abor Volcanics is composed of an alternating sequence of dark grey sandstone to siltstone and green and red shale with rare orthoquartzites and volcanic rocks [Jain and Tondon, 1974]. This formation has been assigned an early to mid-Eocene age on the basis of foraminiferal assemblages [Acharyya, 1994]. The Buxa and Miri formations are intruded by mafic rocks that are exposed in Pangin [Singh, 2012], situated to the west of the Siang Window and the Siang Valley, respectively (Figure 1b).

3. Sampling and petrography

We collected the mafic rocks that intruded in the Buxa Formation of the Pangin area in the Siang window, eastern Himalaya (Figure 1b). Outcrops are 1–2 km long and 500–1000 m wide and show discordant contacts with country rocks. Sampling was done along the road sections of the Rotung–Pangin–Geku section and relatively fresh and unweathered samples were collected (Figure 2a, c) and the coordinates are 28° 13' 54.4" N, 94° 59' 33.5" E. Deformation features and primary flow structures are not observed. There is an increase in grain size from the contact margin to the core of the mafic intrusive bodies. No xenoliths of country rocks were observed in the outcrops, suggesting the intrusive nature of their emplacement. The mafic intrusives are characterized by medium to coarse-grained minerals comprising clinopyroxene (~40–50%) and plagioclase (~50–60%) as the major phases with minor amounts of hornblende, sericite, chlorite and Fe–Ti oxides showing granular textures. Interlocking textures between plagioclase and clinopyroxene were also observed (Figure 2b, d). Clinopyroxene is euhedral to subhedral in shape, has high relief and imperfect cleavages. Plagioclase grains are subhedral to anhedral and short columnar to granular in shape. In some places, the appearance of granophyric textures indicates that the plagioclase has been subject to

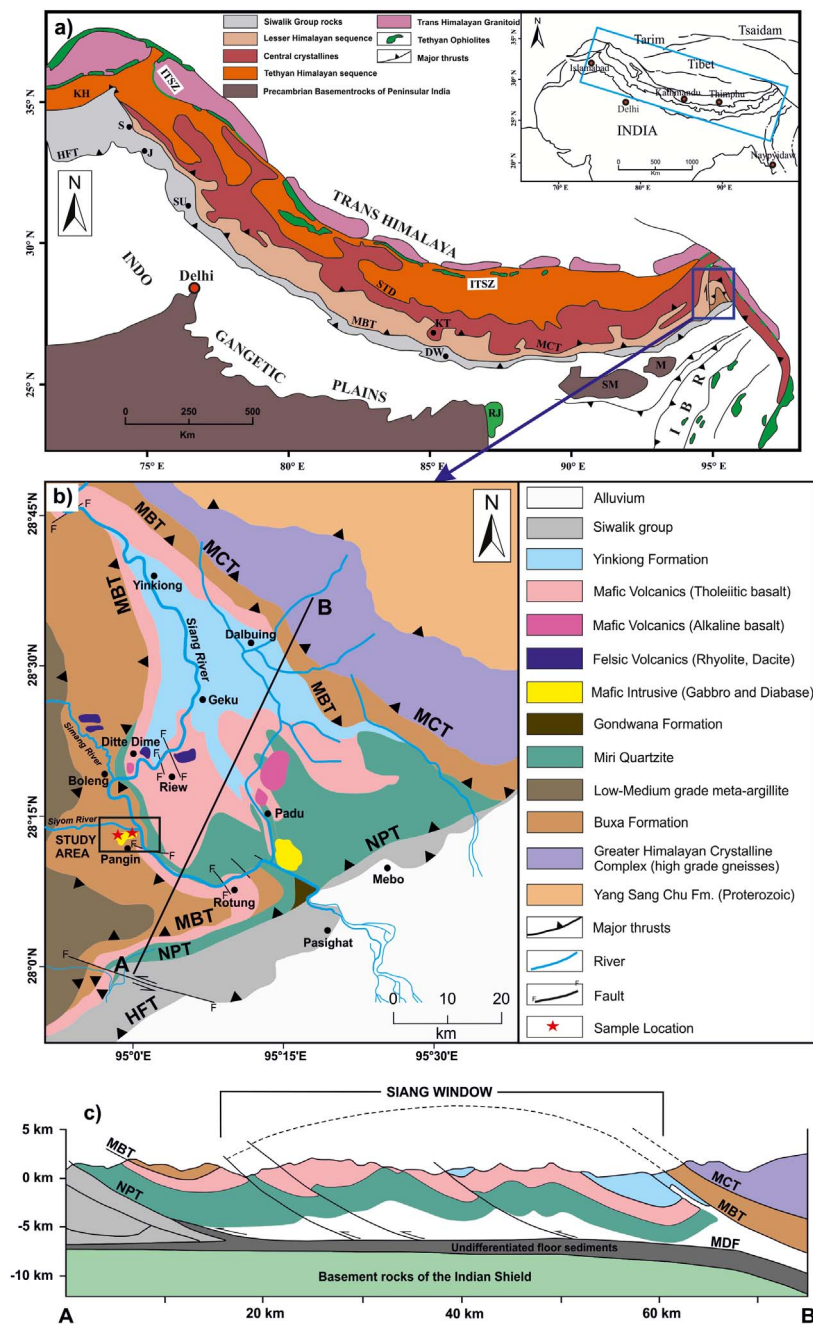


Figure 1. (a) Map showing a broad framework of the Himalaya bounded by major thrusts (modified after Acharyya [2007]); the upper insert shows the location map of the Himalayan mountain range. Abbreviations: KH – Kashmir-Hazara Syntaxis, S – Salal, J – Jammu, SU – Subathu, DW – Dwarkhola, KT – Kathmandu, RJ – Rajmahal Volcanics, SM – Shillong Massif, M – Mikir Massif, IBR – Indo Burma Range, HFT – Himalayan frontal thrust, MBT – Main boundary thrust, MCT – Main central thrust, STD – South Tibetan Detachment and ITSZ – Indus Tsangpo Suture Zone. (b) Geological map of Siang window (modified after Acharyya [2007], Singh and Singh [2012], Singh et al. [2019]); NPT – North Pasighat Thrust. (c) Structural cross-section along AB (modified after Acharyya [2007]); MDF – Main Detachment Fault.

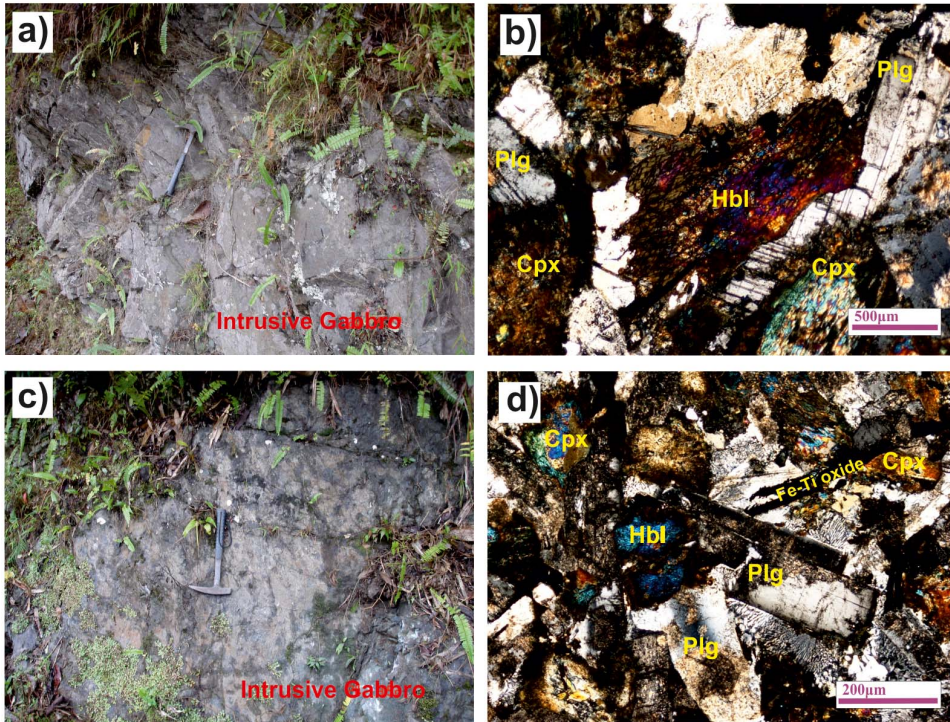


Figure 2. Representative field photographs and photomicrographs of the mafic intrusive rocks from Pangin area of the Siang Window, Eastern Himalaya, Northeast India – (a, c) intrusive medium-grained gabbro in the Buxa formation of Pangin; (b, d) granular and interlocking textures observed in intrusive gabbros with subhedral laths of plagioclase and stumpy clinopyroxene. Abbreviations for minerals are: Cpx – clinopyroxene, Hbl – hornblende, Plg – plagioclase and Fe-Ti oxide – Iron and titanium oxide.

some intergrowth (Figure 2d). All these petrographical observations clearly indicate that the intrusives are primarily gabbroic in nature and have undergone few alterations and low-grade metamorphism which might have caused the formation of hornblende and sericite.

4. Analytical techniques

4.1. XRF-ICPMS – major and trace element analysis

A pressed pellet samples preparation technique was adopted at the Wadia Institute of Himalayan Geology (WIHG), Dehradun, India, to determine the major element and few trace element concentrations for the selected samples using an X-ray Fluorescence Spectrometer (XRF; Bruker, Tiger S8). The analytical methods and data acquisition techniques of Saini *et al.* [2003] was adopted. Approximately 0.5 kg

samples were cut into small chips and then crushed using a steel jaw crusher. In an agate mill, the crushed samples were pulverized up to 200 mesh following which pellets were prepared with approximately 7 g of each powdered sample and then analysed in the XRF. The loss-on-ignition (LOI) was measured after a 5 g sample powder was heated at 1000 °C in a Muffle furnace. The analytical precision is found to be better than $\pm 2\%$ – 3% for major oxides and $\pm 5\%$ – 6% for trace elements.

Rare earth elements (REE) and selected trace element concentrations were analysed using a Perkin-Elmer SCIEX ELAN DRC-e Inductively Coupled Plasma Mass Spectrometer (ICP-MS) at WIHG, Dehradun, India. The analytical procedure of Khanna *et al.* [2009] was adopted. The open-system digestion method was used for the analysis. Approximately 0.1 g of powdered sample was mixed with 20 ml of HF+HNO₃ (2:1 ratio) and ~2 ml of HClO₄ in Teflon crucibles. Then the crucibles were heated

over a hot plate until the samples were fully digested and dried to form a paste. This was followed by the addition of 20 ml of 10% HNO₃ to each sample which was left on a hot plate for 10–15 min until a clear solution was obtained. The clear solution was made up to 100 ml final volume with milli-Q water. BHVO-1 and JB-1a are used as reference standards; their accuracy of trace element ranges from 2% to 12% and precision varies from 1% to 8%. Whole-rock geochemical data of the studied samples are given in Table 1.

4.2. LA-MC-ICPMS – zircon U–Pb geochronology

Zircon grains were separated from two gabbroic samples (GKS-40 and 4X3-A) for the U–Pb geochronology studies. For separation of zircon, the sample was first crushed using a jaw crusher and a disk mill and then sieved up to 60 mesh size. This was followed by gravity separation using the Holman–Wilfley water table, isodynamic magnetic and heavy liquids separation method. Finally, the zircon grains were hand-picked under a binocular microscope at WIHG, Dehradun, India. About 50 zircon grains were mounted in per-fluoro-alkoxy alkane (PFA®) Teflon followed by sequential polishing with 8, 5, 3, 1 and 0.25 µm diamond paste to expose the zircon mid-section. Cathodoluminescence (CL) images of zircon grains were taken on a Zeiss EVO 40 extended pressure (EP) Scanning Electron Microscope (SEM) with a 2 minutes scan time and varying probe current of 10–20 nA.

In situ U–Pb zircon dating was performed by 193 nm excimer laser (UV Laser, Model Analyte G2, Cetec-Photon machine, Inc.), equipped with a high-performance HelEx-II sample chamber and a Multi-Collector Inductively Coupled Plasma Mass Spectrometer (MC-ICP-MS; Neptune Plus, Thermo Fisher Scientific, Inc.) at WIHG, Dehradun, India. The analyses were carried out with a spot diameter of 20 µm (the spots were positioned relative to the CL images), a repetition rate of 5 Hz, an energy density of 4 J/cm² and 75% laser intensity. Instrumental conditions, analysis methods and data acquisition were similar to those described by Mukherjee *et al.* [2017]. For fractionation correction and calculation of results, we used the Z 91500 zircon standard (Thermal Ionization Mass Spectrometry [TIMS] normalization data ²⁰⁶Pb/²³⁸U = 1062.32 ± 2.22 [2 sigma];

Wiedenbeck *et al.* [1995]) and the accuracy was later checked using the Plesovice zircon standard (Isotope Dilution [ID] TIMS ²⁰⁶Pb/²³⁸U age = 337.13 ± 0.37 Ma; Slama *et al.* [2008]) as the external standard. Standards were analysed four times, at the beginning and end of the session, another two analysed after every 10 analyses. Common Pb was corrected following the method of Stacey–Kramers [Stacey and Kramers, 1975]. The isotopic data reductions were processed using Iolite software [Paton *et al.*, 2011]. The Concordia diagrams and U–Pb age calculations were made using *Isoplot R* [Vermeesch, 2018]. The uncertainties of isotopic ratios and ages for a single analytical spot are quoted at 2σ whereas the errors for the weighted average age are given at 2σ (95% confidence). The U–Pb zircon data are given in Table 2.

5. Results

5.1. Whole-rock geochemistry

Geochemical data for the studied gabbros are presented in Table 1. On a nominally anhydrous basis, SiO₂ contents range from 49.39 to 54.95 wt%, Al₂O₃ from 14 to 15.39 wt% and MgO from 5.46 to 7.4 wt%. The samples are characterized by variable Fe₂O₃ (7.09–12.7 wt%) and TiO₂ (0.97–1.93 wt%) contents and are generally sodium-rich (Na₂O > K₂O). They have low and variable Ni (36–63 ppm), Co (29–65 ppm) and Cr (91–169 ppm) values. In the classification diagram of (Na₂O+K₂O) vs. SiO₂ [Cox *et al.*, 1979], the samples plot in the field of gabbro (Figure 3a). All the samples plot within the sub-alkaline basalt field on Nb/Y vs. Zr/Ti diagram (Figure 3b) (after Winchester and Floyd [1977]). On an AFM diagram (Na₂O+K₂O–FeO^l–MgO, after Irvine and Baragar [1971]), they exhibit a typical tholeiitic trend (Figure 3c). The samples show uniform chondrite-normalized rare earth elements (REE) patterns with varying light rare earth elements (LREE) enrichment (La/Yb)_{cn} = 2.65–3.99 and slight Eu anomalies (Eu/Eu* = 1–1.31) (Figure 4a). In the primitive mantle (PM) normalized spider-diagram for incompatible elements, the mafic intrusive rocks exhibit variable abundances. They are enriched in large ion lithophile elements (LILEs) but depleted in high field strength elements (HFSE) (e.g. Hf, Ti, Zr) and are characterized by depleted Nb relative to La (Figure 4b), with Nb/La ratios ranging from 1 to 1.5. They follow a trend similar to E-MORB (Figure 4a, b).

Table 1. Major (wt%) elements and trace elements including rare earth elements (ppm) for the mafic intrusive rocks from Pangin area of Siang Window, Eastern Himalaya, Northeast India

Samples	GK5	GK9	GK13	4X3A	GK8	GK14	GK12	GKS40	4X3B	GKS4	GKS6
SiO ₂	50.81	53.96	54.95	52.28	51.04	52.85	52.85	52.54	50.94	50.50	49.39
TiO ₂	1.60	1.58	0.97	1.51	1.58	1.50	1.53	1.60	1.93	1.93	1.66
Al ₂ O ₃	14.60	14.97	14.04	14.76	14.85	14.71	14.77	15.39	14.00	14.28	14.92
MgO	5.69	6.26	6.50	6.85	5.53	6.55	6.29	7.40	5.46	6.02	6.54
Fe ₂ O ₃	11.19	10.47	7.09	10.76	11.01	10.79	10.66	10.39	12.38	12.70	12.27
CaO	9.64	6.45	9.00	6.23	9.23	6.55	6.46	5.83	8.45	8.90	8.75
K ₂ O	0.38	0.89	0.28	0.93	0.48	1.01	0.88	0.84	0.73	0.75	0.71
Na ₂ O	3.17	3.93	4.48	3.56	3.13	3.53	3.60	3.67	3.18	3.15	3.09
P ₂ O ₅	0.18	0.17	0.11	0.17	0.20	0.17	0.19	0.17	0.26	0.25	0.22
MnO	0.14	0.14	0.07	0.12	0.14	0.11	0.13	0.14	0.16	0.16	0.15
LOI	1.21	2.10	0.88	2.16	0.90	2.08	1.83	2.94	1.04	1.37	2.40
Σ	98.61	100.92	98.37	99.33	98.09	99.85	99.19	100.91	98.53	100.01	100.10
FeO ^t	10.07	9.42	6.38	9.68	9.91	9.71	9.59	9.35	11.14	11.43	11.04
Mg#	50.18	54.22	64.49	55.77	49.87	54.60	53.89	58.52	46.63	48.43	51.36
Trace element (ppm)											
Sc	27	18	45	20	27	21	22	18	28	27	32
V	253	164	356	161	244	164	166	168	272	260	239
Cr	93	78	24	91	169	138	98	97	154	150	109
Co	35	29	18	35	38	35	29	65	39	42	62
Ni	41	51	38	56	41	56	54	63	38	36	38
Ga	21.26	23.34	17.42	22.77	20.84	22.93	22.79	24.64	21.94	23.20	22.20
Rb	6.00	25	4.00	30	9.00	32	26	27	14	14	13
Sr	316	311	153	335	318	359	308	312	292	293	362
Y	22	22	21	24	21	25	23	25	27	30	27
Zr	86	67	113	63	83	63	64	64	105	109	92
Nb	8.10	6.60	7.00	7.10	7.70	6.90	6.90	6.90	9.30	9.50	8.30
Ba	108	167	75	194	115	193	156	143	153	147	152
La	6.53	4.54	13.54	5.05	6.65	5.16	4.90	5.57	7.80	9.20	7.84
Ce	14.99	10.18	27.02	11.28	14.97	11.43	11.06	12.76	18.24	21.86	18.85
Pr	2.33	1.53	3.62	1.69	2.34	1.72	1.70	1.86	2.78	3.27	2.81
Nd	10.69	7.05	14.36	7.88	10.75	8.03	7.75	8.82	12.92	15.40	13.27
Sm	3.23	2.34	3.51	2.68	3.22	2.70	2.58	2.93	3.87	4.72	4.03
Eu	1.29	1.05	1.65	1.21	1.30	1.25	1.15	1.32	1.50	1.68	1.54
Gd	3.86	2.96	4.24	3.38	3.87	3.46	3.27	3.78	4.63	5.63	4.95
Tb	0.63	0.50	0.69	0.56	0.63	0.58	0.55	0.64	0.75	0.92	0.81
Dy	3.68	2.97	4.27	3.36	3.71	3.42	3.29	3.86	4.36	5.45	4.82
Ho	0.73	0.57	0.92	0.65	0.72	0.67	0.63	0.77	0.87	1.10	0.97
Er	1.80	1.39	2.48	1.57	1.84	1.61	1.51	1.84	2.13	2.74	2.42

(continued on next page)

Table 1. (continued)

Samples	GK5	GK9	GK13	4X3A	GK8	GK14	GK12	GKS40	4X3B	GKS4	GKS6
Tm	0.25	0.18	0.36	0.21	0.25	0.21	0.20	0.25	0.29	0.39	0.34
Yb	1.58	1.13	2.43	1.31	1.58	1.34	1.22	1.49	1.83	2.37	2.12
Lu	0.22	0.15	0.36	0.18	0.23	0.18	0.17	0.20	0.27	0.35	0.31
Hf	2.30	1.26	0.62	1.49	2.34	1.56	1.32	1.34	2.82	3.01	2.52
Ta	0.46	0.35	0.42	0.40	0.46	0.24	0.36	0.44	0.59	0.82	0.43
Pb	2.20	17.10	5.50	14.40	2.20	15.40	14.50	22.40	1.10	2.60	1.90
Th	0.51	0.43	3.47	0.44	0.52	0.42	0.41	0.40	0.60	0.69	0.61
U	0.13	0.09	0.47	0.12	0.13	0.10	0.09	0.08	0.14	0.16	0.16
∑REE	51.81	36.54	79.45	41.01	52.06	41.76	39.98	46.09	62.24	75.08	65.08
LREE	39.06	26.69	63.70	29.79	39.23	30.29	29.14	33.26	47.11	56.13	48.34
HREE	12.75	9.85	15.75	11.22	12.83	11.47	10.84	12.83	15.13	18.95	16.74
(Nb/La) _N	1.20	1.40	0.50	1.35	1.12	1.29	1.36	1.19	1.15	0.99	1.02
(Ta/La) _N	1.18	1.29	0.52	1.33	1.16	0.78	1.23	1.32	1.27	1.49	0.92
(Hf/Sm) _N	1.02	0.77	0.25	0.80	1.04	0.83	0.73	0.66	1.05	0.91	0.90
(La/Yb) _{cn}	2.96	2.88	4	2.77	3.02	2.76	2.88	2.68	3.06	2.78	2.65
(Gd/Yb) _{cn}	2.02	2.17	1.44	2.13	2.03	2.14	2.22	2.10	2.10	1.97	1.93
(Sm/Yb) _{cn}	2.27	2.30	1.60	2.27	2.26	2.24	2.35	2.18	2.35	2.21	2.11
Eu/Eu*	1.12	1.22	1.31	1.22	1.12	1.25	1.21	1.21	1.08	1.00	1.05

Mg# = $100 \times (\text{MgO}/40.304)/(\text{MgO}/40.304 + \text{FeO}/71.839)$; $\text{Eu}/\text{Eu}^* = (\text{Eu})_{\text{cn}}/((\text{Gd}_{\text{cn}} + \text{Sm}_{\text{cn}})/2)$; cn-chondrite; N-primitive mantle normalized. The FeO^{t} values are recalculated based on the analysed $\text{Fe}_2\text{O}_3^{\text{t}}$ values: $\text{FeO}^{\text{t}} = 0.8998 \times \text{Fe}_2\text{O}_3^{\text{t}}$.

5.2. Zircon U–Pb geochronology

Zircons in samples GKS-40 are colourless to translucent, euhedral to subhedral in shape, ~80–200 μm long with length to width ratios varying from 2:1 to 3:1. In CL images, most zircon grains show clear oscillatory zoning and few grains show thin bright overgrowth rims (Figure 9a). A total number of sixteen spots were analysed on 15 zircon grains from this sample. The analytical data show a wide range of Pb (15.5–100.9 ppm), U (40.5–696 ppm) and Th (63.1–517 ppm) with Th/U ratios of 0.12–3.30 (Table 2). The CL images of zircon grains together with their high Th/U ratios imply a magmatic origin [Hoskin and Black, 2000]. Out of the 16 zircon spots analysed, ten spots give $^{206}\text{Pb}/^{238}\text{U}$ concordia age of 568 ± 2 Ma (Figure 10a; MSWD = 0.0071), which can be considered to represent the magmatic event during the Late Proterozoic (Ediacaran).

Zircons in sample 4X3-A are colourless or pale

brown and transparent. The anhedral to subhedral grains show a near-prismatic or irregular morphology with a length of 50–200 μm and length to width ratios varying from 1:1 to 3:1. In CL images, most zircon grains show clear oscillatory zoning, and few grains show thin bright overgrowth rims (Figure 9b), which indicate magmatic origin. A total of 14 spots were analysed on 13 zircon grains from this rock. The analytical data show a high range of Pb (10–88.8 ppm), U (87.4–1250 ppm) and Th (25.8–321 ppm) with Th/U ratios of 0.13–1.42 (Table 2). Eight analysed zircon spots define concordia $^{206}\text{Pb}/^{238}\text{U}$ age of 521.50 ± 3 Ma (Figure 10b; MSWD = 0.0011), which can be further considered to either represent an early Cambrian magmatic event or might be a part of the same magmatic event as that determined from GKS-40, which might have lasted for 40 Ma. Th/U vs. U plots (Figure 9c, d) indicate that the zircon grains from both samples have a magmatic origin.

Table 2. LA-MC-ICPMS zircon U–Pb ages of the gabbro samples (GKS-40 and 4X3-A) from the Siang Window, Northeast India

Spots	Element content (ppm) Th/U			Isotope ratio ($\pm 2\sigma$)						Age (Ma $\pm 2\sigma$)						
	Th	U	Pb	$^{207}\text{Pb}/^{206}\text{Pb}$		$^{207}\text{Pb}/^{235}\text{U}$		$^{206}\text{Pb}/^{238}\text{U}$		$^{207}\text{Pb}/^{206}\text{Pb}$		$^{207}\text{Pb}/^{235}\text{U}$		$^{206}\text{Pb}/^{238}\text{U}$		
	ppm	ppm	ppm	Ratio	$\pm 2\sigma$	Ratio	$\pm 2\sigma$	Ratio	$\pm 2\sigma$	Age (Ma)	$\pm 2\sigma$	Age (Ma)	$\pm 2\sigma$	Age (Ma)	$\pm 2\sigma$	
Sample GKS-40: Gabbro, Lat. 28° 13' 54.4" N, Lon. 94° 59' 33.5" E, Concordia age of 10 spots = 567.66 \pm 2.09 Ma (MSWD = 0.0071)																
GKS-40-1	317	376	15.5	0.84	0.0481	0.0004	0.140	0.005	0.0211	0.0007	101	18	133	4	134	4
GKS-40-2	127	669	33.5	0.19	0.0580	0.0003	0.663	0.008	0.0826	0.0010	528	9	516	4	511	5
GKS-40-3	138	194	28.1	0.71	0.0578	0.0003	0.670	0.017	0.0837	0.0019	522	12	520	10	518	11
GKS-40-4	517	342	95	1.51	0.0575	0.0005	0.669	0.024	0.0867	0.0028	508	17	522	14	535	16
GKS-40-5	349	651	68.3	0.54	0.0579	0.0003	0.714	0.013	0.0889	0.0016	526	11	547	7	548	9
GKS-40-6	322	416	57.7	0.77	0.0579	0.0005	0.734	0.016	0.0920	0.0017	527	19	560	9	567	9
GKS-40-7	130	241	28.7	0.54	0.0567	0.0002	0.722	0.010	0.0922	0.0013	478	6	552	6	568	7
GKS-40-8	63.1	279	17.9	0.23	0.0617	0.0022	0.753	0.022	0.0886	0.0030	650	70	570	12	547	18
GKS-40-9	81.7	696	17.08	0.12	0.0593	0.0003	0.760	0.010	0.0927	0.0012	579	10	574	5	571	6
GKS-40-10	132.9	260	29.4	0.51	0.0581	0.0006	0.746	0.021	0.0926	0.0018	532	21	565	12	570	11
GKS-40-11	238	146	49.3	1.63	0.0574	0.0002	0.741	0.011	0.0933	0.0013	506	7	562	6	574	7
GKS-40-12	133.8	40.5	28.79	3.30	0.0649	0.0031	0.843	0.051	0.0939	0.0011	740	86	617	26	578	6
GKS-40-13	169	535	38.6	0.32	0.0648	0.0010	0.875	0.055	0.0949	0.0059	765	30	633	31	583	35
GKS-40-14	201	512	55.1	0.39	0.0632	0.0011	0.926	0.032	0.1103	0.0039	701	31	664	17	674	23
GKS-40-15	236	217	100.9	1.09	0.0714	0.0004	1.675	0.029	0.1725	0.0022	967	11	998	11	1026	12
GKS-40-16	138.1	244.1	65.8	0.57	0.0751	0.0002	2.177	0.020	0.2091	0.0020	1072	4	1173	6	1224	11
Sample 4X3-A: Gabbro, Lat. 28° 13' 55.7" N, Lon. 94° 59' 39.2" E, Concordia age of 08 spots = 521.50 \pm 2.53 Ma (MSWD = 0.0011)																
4X3-A-1	321	1250	50.2	0.26	0.0651	0.0007	0.482	0.014	0.0532	0.0015	775	21	400	9	334	9
4X3-A-2	178	339.7	35.4	0.52	0.0565	0.0002	0.599	0.016	0.0770	0.0023	473	8	476	10	478	14
4X3-A-3	301	567	61	0.53	0.0595	0.0011	0.653	0.022	0.0808	0.0020	579	38	509	13	501	12
4X3-A-4	163	717	32.6	0.23	0.0590	0.0003	0.679	0.013	0.0829	0.0017	566	12	525	8	513	10
4X3-A-5	86.8	574	18.2	0.15	0.0570	0.0003	0.661	0.010	0.0839	0.0015	489	13	515	6	519	8
4X3-A-6	220	185	45	1.19	0.0564	0.0003	0.652	0.009	0.0839	0.0010	468	11	509	5	519	6
4X3-A-7	135	626	28.5	0.22	0.0582	0.0003	0.689	0.012	0.0853	0.0014	535	11	531	7	527	8
4X3-A-8	281	416	56.6	0.68	0.0586	0.0005	0.691	0.015	0.0852	0.0015	549	17	532	8	526	9
4X3-A-9	232	462	53.5	0.50	0.0626	0.0026	0.704	0.023	0.0867	0.0018	649	69	540	14	536	11
4X3-A-10	38	145	10	0.26	0.0734	0.0085	0.885	0.097	0.0876	0.0046	860	170	632	51	541	27
4X3-A-11	297	1040	75	0.29	0.0615	0.0010	0.816	0.039	0.0955	0.0052	651	34	603	21	587	30
4X3-A-12	46.2	360	13.47	0.13	0.0629	0.0007	0.915	0.047	0.1053	0.0043	702	25	655	25	645	25
4X3-A-13	108	178	52.7	0.61	0.0750	0.0005	2.132	0.029	0.2074	0.0022	1068	13	1158	9	1215	12
4X3-A-14	124	87.4	88.8	1.42	0.1009	0.0005	4.245	0.041	0.3064	0.0027	1641	9	1685	6	1723	13

Note: Indicated by bold is used for Concordia diagram.

6. Discussion

6.1. Fractional crystallization and crustal contamination

Before considering any petrogenetic interpretation, it is important to evaluate the effects of metamorphism and alteration on the geochemistry of any mafic

magmatic rocks. The studied samples have not undergone significant secondary alteration as inferred from their low LOI values (LOI = 0.88–2.94 wt%), absence of Ce anomalies, and lack of carbonization or silicification. In mafic rocks, LILE such as Sr, Ba and Rb are considered as mobile elements, while transition elements such as Ni, Cr and V and HFSE such as REE, Nb, Ti and Th as immobile during alteration and

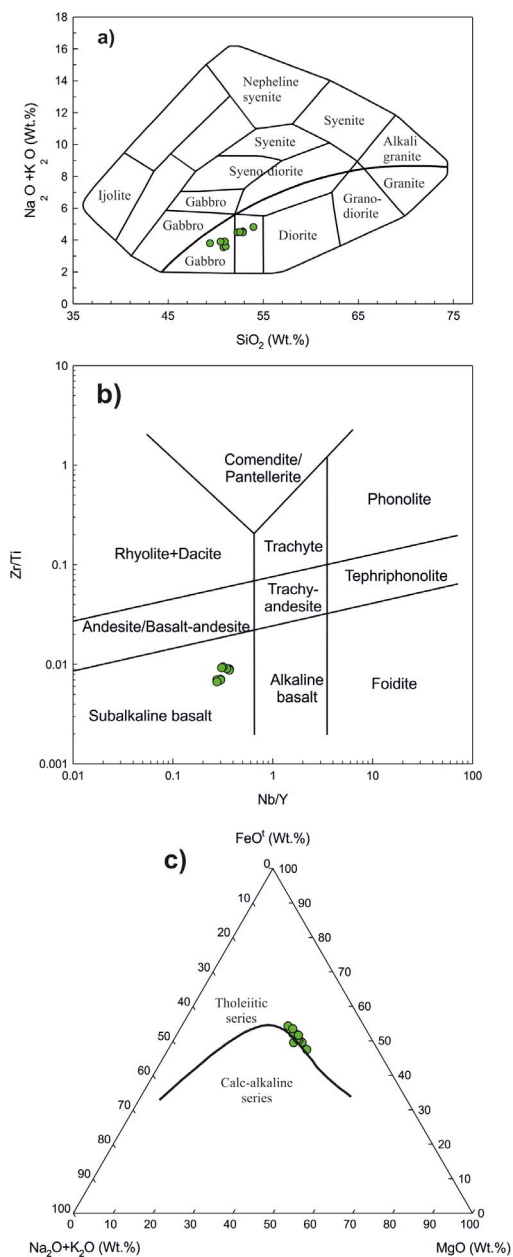


Figure 3. (a) SiO_2 vs. $\text{Na}_2\text{O} + \text{K}_2\text{O}$ (after Cox *et al.* [1979]); (b) Nb/Y vs. Zr/Ti (after Winchester and Floyd [1977]); (c) AFM diagram indicating tholeiitic signature (after Irvine and Baragar [1971]) for the mafic intrusive rocks from Pangin area of Siang Window.

low-grade metamorphism [Pearce and Cann, 1973, Staudigel *et al.*, 1996]. Zr is regarded as the most im-

mobile element under the lower grade of metamorphism [Pearce and Peate, 1995, Polat *et al.*, 2002] and is used as an alteration index during geochemical variations [Liu *et al.*, 2012, Pearce *et al.*, 1992]. In this study, there is a positive correlation between Zr and REE, Hf, Ta, Nb and U which indicates that they are not mobilized during alteration and metamorphism (see Table 1). Therefore, only HFSE and immobile elements are used for the studies of the petrogenesis and tectonic environment of the mafic intrusive rocks.

The low MgO (<8 wt%), Ni (36–63 ppm) and high Mg# (46.63–64.49) contents in these rocks point towards an evolved nature of the parent magma that underwent varying degrees of fractional crystallization and/or crystal accumulation. Positive correlations between Mg# and Ni and Cr indicate crystal fractionation of olivine and pyroxene, whereas negative correlations between V, TiO_2 and Fe_2O_3 vs. Mg# suggest a minimum accumulation of amphibole and late-stage crystallization of Fe–Ti oxides in the magma (see Table 1; figure not shown). In addition, positive trends between Mg# and Al_2O_3 and weak Eu anomalies ($\text{Eu}/\text{Eu}^* = 1\text{--}1.31$) in the samples indicate that they record negligible plagioclase fractionation.

Crustal contamination is a common feature for mantle-derived magmas inside the magma chamber or during ascent which leads to changes in the major oxide and trace element concentrations of mafic rocks [DePaolo, 1981]. Such contaminated rocks show enrichment of LREEs, LILEs, negative Nb, Ta, Ti anomalies and positive Zr–Hf anomalies in their primitive mantle normalized patterns (e.g. Rudnick and Gao 2003, Zhao and Zhou 2007). In this study, we did not observe a strong depletion of Zr–Hf, Nb–Ta and Ti (Figure 4b), which indicates minimum crustal contamination during the evolution of the studied rocks. This observation is also supported by the lack of correlation between SiO_2 and $(\text{Th}/\text{Nb})_{\text{PM}}$ (Figure 5a). $(\text{La}/\text{Nb})_{\text{PM}}$ vs. $(\text{Th}/\text{Nb})_{\text{PM}}$ diagrams (Figure 5b) also suggests insufficient input of continental crust. Contamination of Th and U in the middle and upper crust causes their amounts to increase rapidly in the ascending magma [Taylor and McLennan, 1985], but these features are not observed in the studied samples. To summarise, crustal contamination is considered to be negligible for the parental magmas of the studied samples. The slight enrichment of LREE reflects the charac-

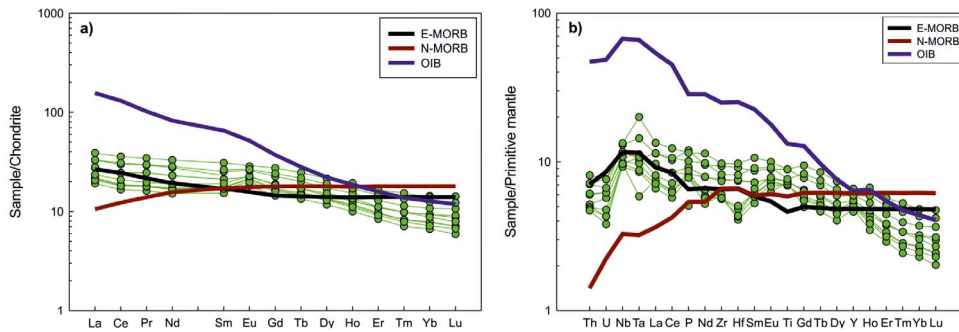


Figure 4. Chondrite-normalized REE pattern (a) and primitive mantle-normalized trace element pattern (b) for the mafic intrusive rocks from the Pangin area of the Siang Window. The normalizing values for chondrite and primitive mantle are from Sun and McDonough [1989]. Data for OIB, E-MORB and N-MORB are also from Sun and McDonough [1989].

teristics of the source mantle prior to magma extraction. Therefore, the whole rock geochemical composition of the studied gabbros are of pure magmatic origin with little signs of contamination and can be used to determine the mantle source of the magmas as well as the processes that occurred during their emplacement.

6.2. Mantle source characteristics

The HFSE and LREE ratios (Nb/Ta, Zr/Hf and Nb/Yb) are important proxies for identifying different sources of the mantle for mafic magmatic rocks [Pearce and Peate, 1995, Weyer *et al.*, 2003]. In our study, the gabbros show higher LREE and HFSE enrichment and Nb/Ta (15.68–28.75) and Zr/Hf (35.47–53.17) ratios higher than the chondritic values (17.6, 36.3, respectively) suggesting their generation from an enriched mantle source [Weyer *et al.*, 2003]. Th/Nb vs. Nb/Yb, and TiO₂/Yb vs. Nb/Yb plots (Figure 6a, b) confirm the enriched mantle source signature of the studied samples. The absence of strong negative Nb–Ta and Zr–Hf anomalies in the primitive mantle normalized diagram (Figure 4b) combined with their plotting in the MORB–OIB array (Figure 6a) indicates that these rocks do not record any interaction with slab-derived material [Pearce, 2008]. The samples have high La/Yb and Nb/La ratios (3.70–5.57 and 0.52–1.45) and fall in the asthenospheric mantle source field (Figure 7) suggesting that they are not contaminated by crustal rocks. The studied rocks have higher Th/Yb (0.27–1.43), Th/Ta (0.84–1.75), Ta/Yb (0.17–0.35) and Zr/Y (2.53–5.38) ratios

and lower Zr/Nb (8.87–16.14) and La/Nb (0.69–0.97) ratios as compared to normal-MORB (0.04, 0.75, 0.052, 2.64, 31.75 and 1.07, respectively; after Sun and McDonough [1989]). These geochemical ratios are clear indications towards an E-MORB source.

Primitive normalized spider diagrams and chondrite normalized REE patterns of the studied samples show a pattern similar to E-MORB (Figure 4a, b). There is a slight depletion of Ti and Nb anomalies in comparison to La and Ce (Figure 4b). Their insignificant Eu anomalies indicates that plagioclases were not fractionated (Figure 4a). Zr/Ba ratio is regarded as a geochemical signature for differentiating between the asthenospheric source (Zr/Ba > 0.5) and lithospheric source (0.3–0.5) K rk c ođlu [2010], Menzies *et al.* [1991]. In this study, the Zr/Ba ratio ranges from 0.32 to 1.51 and the Zr/Hf ratios vary between 35.47 and 53.17 indicating an asthenospheric source. This observation is also supported by Nb/La vs. La/Yb (Figure 7), where the studied samples fall in the asthenospheric mantle.

To understand the melting conditions of the mantle, REE compositions are treated as a geochemical signature because the REE ratios can indicate the degree of partial melting [He *et al.*, 2010, Lassiter *et al.*, 1995, Reichow *et al.*, 2005]. In the spinel stability field, Sm/Yb is unfractionated while La/Yb is somewhat fractionated; for the garnet peridotite field, both Sm/Yb and La/Yb are strongly fractionated [Lai *et al.*, 2012, Xu *et al.*, 2005, Yaxley, 2000]. The studied gabbros are marked by (La/Yb)_{CN} = 2.65–3.99, (Sm/Yb)_{CN} = 1.60–2.35 and (Gd/Yb)_{CN} = 1.44–2.22

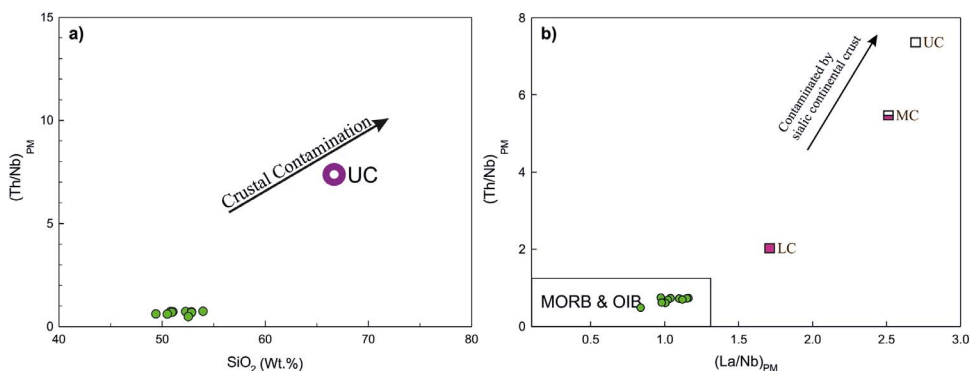


Figure 5. (a) SiO_2 vs. $(\text{Th}/\text{Nb})_{\text{PM}}$; (b) $(\text{La}/\text{Nb})_{\text{PM}}$ vs. $(\text{Th}/\text{Nb})_{\text{PM}}$ (after Frey *et al.* [2002]) plots for testing crustal contamination of mafic intrusive rocks from the Pangin area of the Siang Window. Subscripts PM indicate ratios normalized to primitive mantle values of Sun and McDonough [1989]. UC-upper crust, MC-middle crust, and LC-lower crust values after Rudnick and Gao [2003].

(see Table 1) indicating moderate fractionation of HREE which suggest that the source magma might have both garnet and spinel peridotite components [Buslov *et al.*, 2010, Safonova *et al.*, 2008]. In Figure 8a (La/Sm vs. Sm/Yb plot), the studied samples fall in the garnet peridotite trend. In Sm/Yb vs. Sm plot (Figure 8b), the samples fall between the field of garnet and spinel-garnet lherzolite. Mafic lavas are considered to be derived from mantle melting at depths less than 100 km. Generally, the mantle source of this field is considered to be at a depth between 60 and 80 km but in case of the presence of a mantle plume, their depth might be 80–100 km [McKenzie and O’Nions, 1991, White and McKenzie, 1995]. Therefore, it is suggested that the studied gabbros of the Siang window, eastern Himalaya, were produced by 12–28% partial melting of a mantle source extending from spinel+garnet lherzolite to garnet lherzolite facies at a depth of 60–100 km.

The origins of mafic magmatic rocks are mainly ascribed to: (1) within-plate oceanic or continental environments, (2) fast and slow-rifting MORs, (3) island arcs and (4) back-arc basins [Pearce, 2008, Pearce and Cann, 1973, Pearce and Norry, 1979]. The studied samples consist of low to medium Ti contents ($\text{TiO}_2 = 0.97\text{--}1.93$ wt%), $\text{Al}_2\text{O}_3/\text{TiO}_2$ ranging from 7.25–14.47 and are compared to island arc basalts (15–25) and MORB (10–15), thus suggesting their formation within a plate oceanic or continental tectonic environment [Manikyamba *et al.*, 2004, Regelous *et al.*, 2003]. To classify basaltic magmas

generated in different tectonic environments, Sacconi [2015] has used the Th and Nb systematics (Figure 11a). On Th_N vs. Nb_N plot (Figure 11a), the studied samples fall near the back-arc B field which indicates that subduction-derived fluids or any other crustal components have not played any role in the formation of our rocks. This type of tectonic setting is usually found in mature intra-oceanic or intra-continental back-arcs. In the tectonic discrimination diagram of V vs. Ti (Figure 11b), the mafic intrusives are plotted in MORB and continental flood basalts (CFB) field and possess high Ti/V ratios. The Zr vs. Zr/Y diagram of Pearce and Norry [1979] helps in effectively discriminating between basalts from different tectonic settings like oceanic-island arc, mid-oceanic ridges, within-plate and back-arc, and our samples plot in the zone of within-plate basalts (WPB) and MORB (Figure 11c). In the plot of Zr vs. Ti (Figure 11d), the studied samples fall in the field of within plate basalts (WPB) and MORB, further proving their intra-continental geodynamic setting. WPBs which have higher Ti/Y and Nb/Y ratios signify an enriched mantle source relative to N-MORB and volcanic arc basalts (VABs) [Rollinson, 1993]. The absence of primary hornblende in thin sections, enriched LREEs and low to moderate concentration of Ti in the samples also suggest an E-MORB source for the studied rocks. Keeping all these arguments in mind, it can be suggested that the mafic intrusives (gabbros) of the Siang window originated in a continental extension environment.

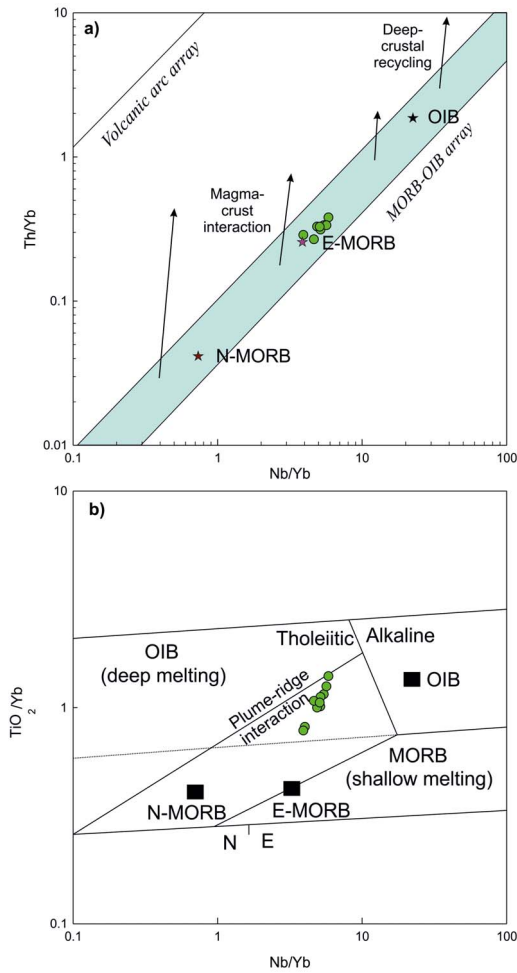


Figure 6. (a) Nb/Yb vs. Th/Yb plot (after Pearce [2008]); (b) Nb/Yb vs. TiO₂/Yb diagram (after Pearce [2014]) for mafic intrusive rocks from the Pangin area of the Siang Window. Data for E-MORB, N-MORB, and OIB are from Sun and McDonough [1989].

6.3. Geodynamic implications

Earlier, it has been proposed that the Abor volcanism was contemporaneous to the Indian and Eurasian plates collision event which occurred during the Early Eocene due to either adiabatic decompression following thickening of the crust [Sengupta et al., 1996] or a thermal anomaly caused by slab break-off following the collision [Acharyya, 2007]. Later, K/Ar dating for the Abor volcanics on different basalt samples yielded varied ages of 319

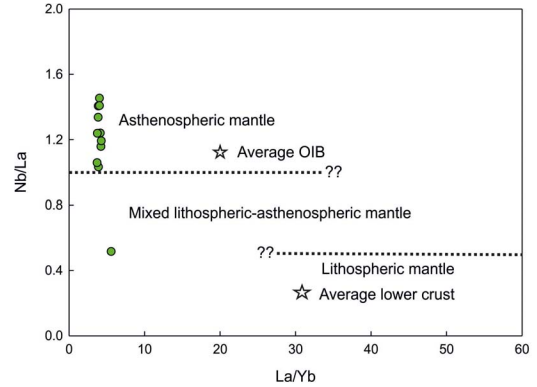


Figure 7. La/Yb vs. Nb/La plot to distinguish for the lithospheric and asthenospheric mantle (after Abdel-Rahman and Nassar [2004]) for mafic intrusive rocks from the Pangin area of the Siang Window.

± 15 Ma (Late Carboniferous), 87.2 ± 1.3 (Late Cretaceous) and 24.9 ± 0.4 Ma (Early Tertiary) [Liebke et al., 2011]. Ali et al. [2012] have interpreted the steeply dipping magnetization in the basalts to be primary in nature and have given them a Permian age. They have deduced that the rocks formed due to eruptions associated with rifting of blocks of the Cimmerian continent situated in the northern margin of the Gondwana supercontinent. More recently, zircon U–Pb geochronological studies of the Abor volcanics suggest that they were emplaced due to the outburst of the Kerguelen plume at the early stages (~132 Ma) of the eastern Gondwana breakup [Singh et al., 2019].

In light of the recent findings, our zircon U–Pb data for the mafic intrusive rocks from the Pangin area of the Siang window yield an age ranging from 521 to 567 Ma, i.e. Late Neoproterozoic to Early Cambrian which is the oldest magmatic event reported so far from the Siang window. This age coincides with the age of the closing of the Mozambique Ocean during the Kuunga orogeny which is the eastern part of the Pan-African orogenic belt [Meert, 2003, Meert and Lieberman, 2008]. Our obtained ages are totally different from the previous studies; therefore, their source might also be different from the Abor Volcanics.

It has been reported that the Himalayan lithotectonic units were part of the north Indian passive margin from the Precambrian to the Cretaceous pe-

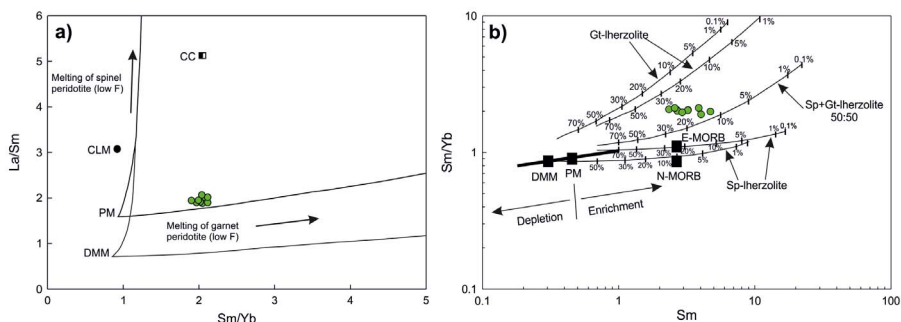


Figure 8. (a) Sm/Yb vs. La/Sm plot for the mafic intrusive rocks from the Pangin area of the Siang Window. Batch melting trends for garnet and spinel peridotite are after Lassiter and DePaolo [1997]. Arrows denote the effect of decreasing melt fraction (F). (b) Plots of Sm/Yb vs. Sm for the mafic intrusive rocks from the Pangin area of the Siang Window, Eastern Himalaya, Northeast India. The heavy line represents the mantle array defined using DMM [McKenzie and O’Nions, 1991] and PM compositions [Sun and McDonough, 1989]. N-MORB and E-MORB compositions are from Sun and McDonough [1989]. Solid curves (or lines) are the melting trends from DMM. Melting curves for spinel Iherzolite ($Ol_{53} + Op_{x27} + Cpx_{17} + Sp_{11}$) and garnet peridotite ($Ol_{60} + Op_{x20} + Cpx_{10} + Gt_{10}$) with both DMM and PM compositions are after Aldanmaz *et al.* [2000]. Number marks on each curve (or line) correspond to degrees of partial melting for a given mantle source.

riod [Brookfield, 1993]. This observation is inconsistent with the presence of many early Paleozoic granites in the Himalaya [Nadimi, 2007, Ramezani and Tucker, 2003]. It has been also reported that from 500 to 475 Ma, the Kathmandu region of the Higher Himalayan crystalline underwent deformation and that the Indian proto-Tethyan margin was strongly affected during the Cenozoic Himalayan formation [Cawood *et al.*, 2007, Gehrels *et al.*, 2006]. During the assembly of the Gondwana supercontinent (570–510 Ma), the initiation of subduction along the Gondwana proto-Tethyan and Gondwana proto-Pacific margins occurred in the last stage of subduction [Cawood and Buchan, 2007, Cawood *et al.*, 2007]. From this observation, Cawood *et al.* [2007] interpreted the early Paleozoic magmatism found in the Himalaya as the result of southward subduction of the proto-Tethyan oceanic lithosphere beneath the northern Indian continent. Similar Late Neoproterozoic to Early Cambrian magmatisms are also reported from the northern Gondwana margin of Australia, Iran, Arabia and Turkey, which is shown in Figure 12 [Gürsu and Göncüoğlu, 2005, Gürsu *et al.*, 2015, Hassanzadeh *et al.*, 2008, Horton *et al.*, 2008, Mahmoud *et al.*, 2011, Saki, 2010, Ramezani and Tucker, 2003].

A late Pan-African granitic activity (500 ± 50 Ma) and a transgressive Ordovician sedimentary succession characterize a large area of the Indian part of the Gondwana supercontinent [Le Fort *et al.*, 1994]. Gaetani and Garzanti [1991] proposed that the early Paleozoic granitoids might have been associated with the formation of the Gondwana supercontinent. Based on geochemical characteristics, and ages (absence of Sr and Ba enrichment; the short-lasting magmatism from 550 to 470 Ma; in the absence of Cambro-Ordovician metamorphic and deformation records) of the Mandi basalts in northwest Himalaya, it has been proposed that the Mandi magmatism was emplaced in an extensional tectonic setting rather than a subduction to collision-related setting [Debon *et al.*, 1986, Le Fort *et al.*, 1986, Miller *et al.*, 2001]. Further, Miller *et al.* [2001] have also proposed that the Mandi basalts were formed due to the asthenospheric upwelling and passive crustal extension possibly in a rift setting that separated the proto-Indian margin and the cratonic Asian fragments such as the South China block [Dalziel *et al.*, 1994]. They also correlate the early Paleozoic magmatic activities from the northwest Himalaya with the late extensional stage of the long-lasting Pan-African orogenic events which ended with the formation of the Gondwana super-

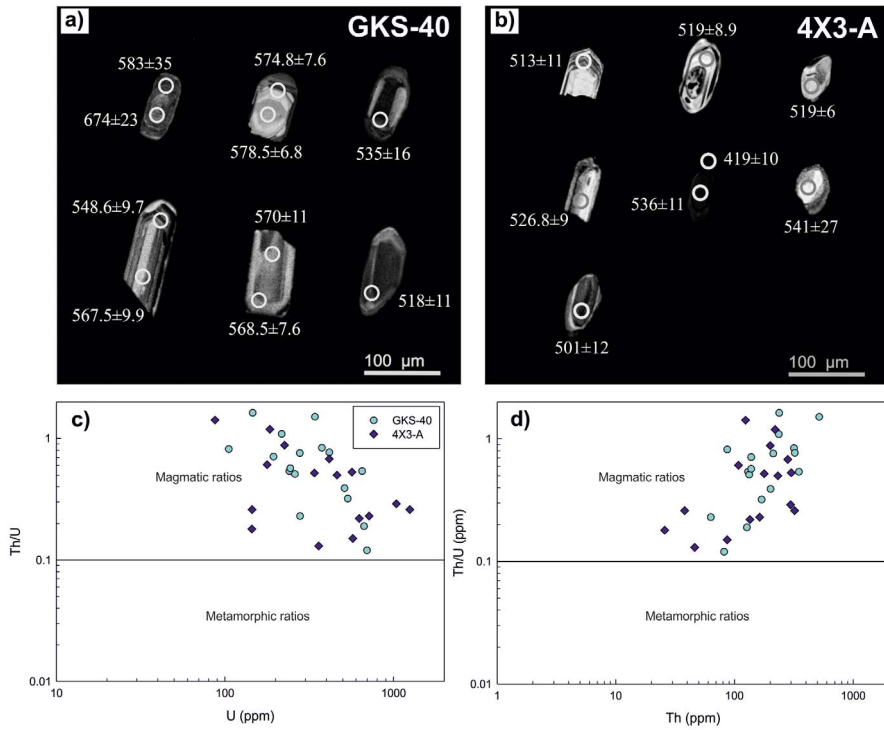


Figure 9. Cathodoluminescence (CL) images (a, b) of zircon U–Pb dating for the mafic intrusive rocks from the Pangin area of Siang window. U vs. Th/U and Th vs. Th/U plots (c, d) (after Hoskin and Black [2000]).

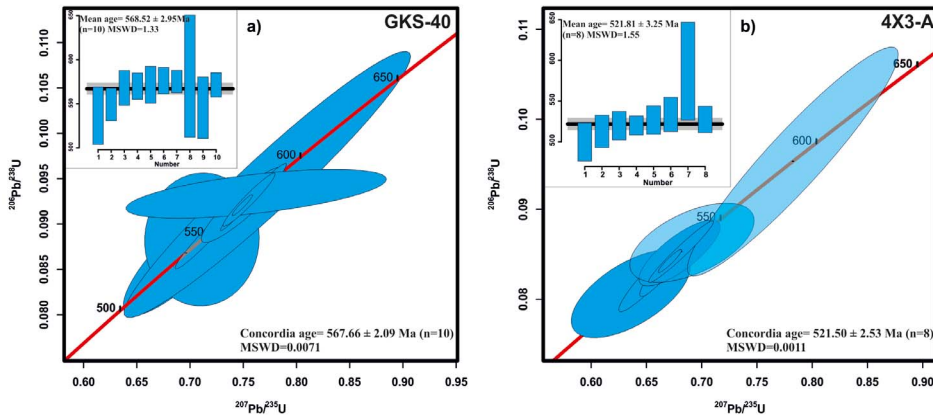


Figure 10. Concordia plots of zircon U–Pb dating for the mafic intrusive rocks: (a) Sample GKS 40, (b) Sample 4X3-A from the Pangin area of the Siang Window; the upper insert shows the weighted mean age.

continent [Girard and Bussy, 1999]. The early Palaeozoic granites in the Northwest Himalaya post-date the collision and other major thermal events dur-

ing the Pan-African orogeny. Palaeogeographic reconstructions suggest that only the southern parts of the Indian plate were affected by the main Pan-

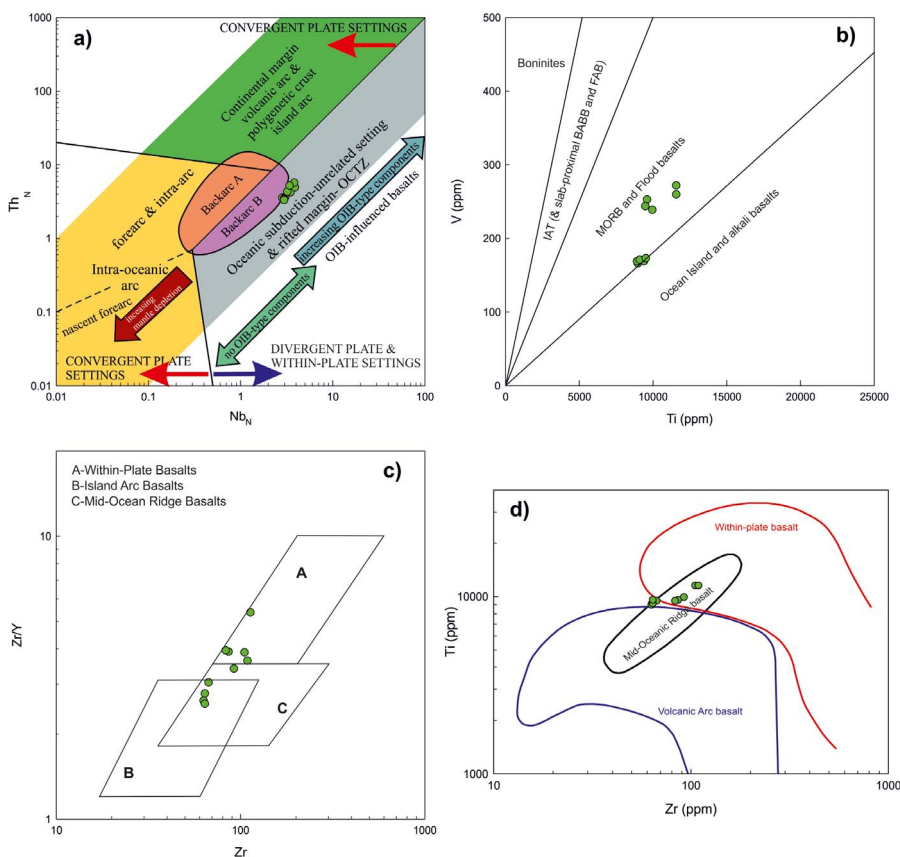


Figure 11. Tectonic discrimination diagrams for mafic intrusive rocks from the Pangin area of the Siang window (a) Nb_N vs. Th_N (after Saccani [2015]); N – normalizing values are the N-MORB composition of Sun and McDonough [1989]; (b) V vs. Ti plot (after Shervais [1982]) showing that the studied samples fall in the field of MORB and flood basalts; (c) Zr/Y vs. Zr diagram (after Pearce and Norry [1979]); (d) Ti vs. Zr (after Pearce *et al.* [1981]).

African event (e.g. Stern 1994). Therefore, the faults bounding the vast infra-Cambrian to mid-Cambrian evaporite basins of central Iran could have been related to a late Pan-African Basin-and-Range type rift cluster that may have affected much of the Gondwana margin between Arabia and northern India [Sengör and Natal'in, 1996]. Since the magmatic arc is absent in the present study area, we have ruled out the formation of the studied mafic intrusive rocks in the BABB setting as this is geologically invalid, but we have compared them to the late extensional stage of the long-lasting Pan-African orogenic cycle in the northern Indian Gondwana margin, which ended with the assembly of the Gond-

wana supercontinent. Compared with the previously reported emplacement of numerous Late Neoproterozoic to Early Cambrian granitoids and Early Paleozoic mafic rocks of northwest Himalaya, our data also represent an extensional environment of the northern Gondwana margin related to the late extensional stage of the Pan-African orogenic cycle with the formation of the Gondwana supercontinent. A Late Neoproterozoic-Early Cambrian reconstruction depicting the location of peri-Gondwana terranes with the present investigated mafic intrusive rocks along the northern margin of the Gondwana supercontinent is shown in Figure 12 (modified after Zhu *et al.* [2012]).

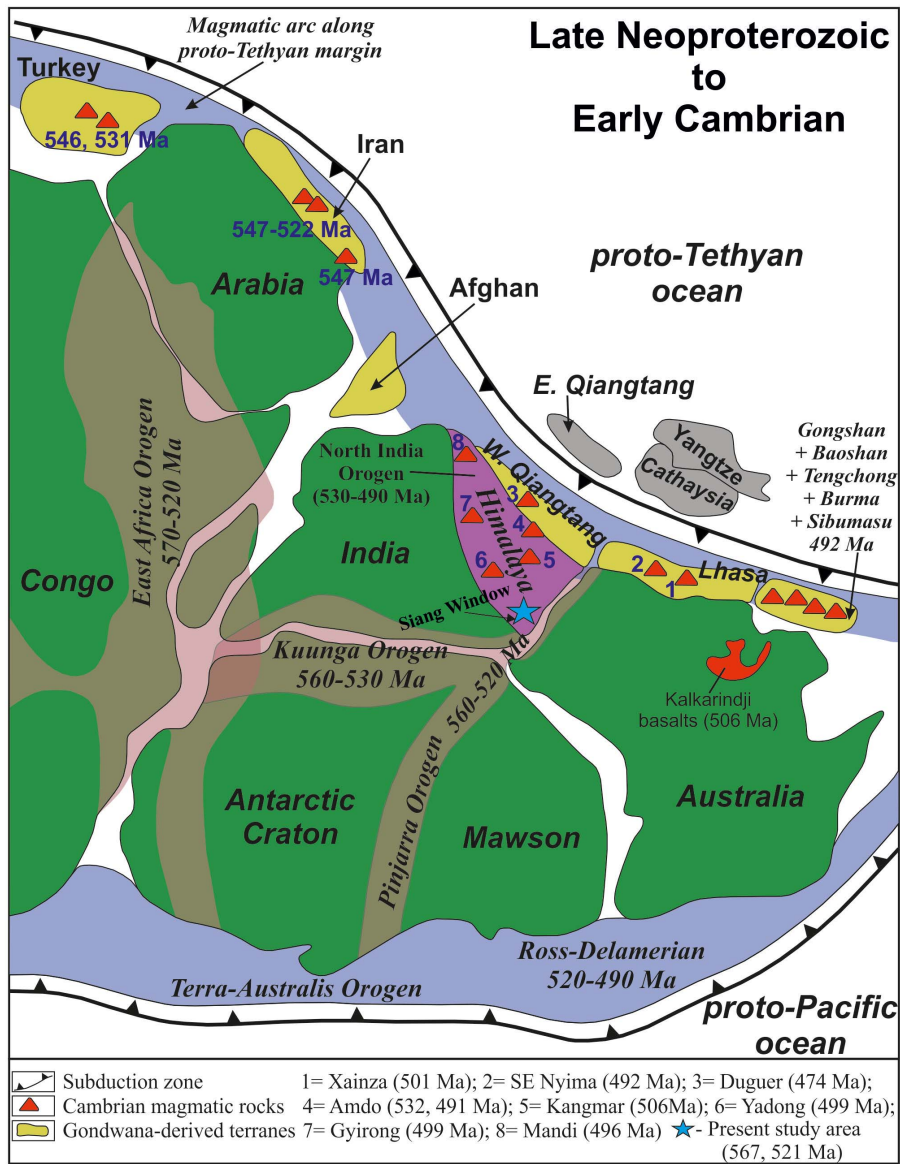


Figure 12. Reconstruction of the northern margin of Gondwana (modified from Zhu et al. [2012]) showing the location of the proposed late Neoproterozoic to early Cambrian extensional tectonic environment and early Paleozoic Andean-type magmatic arc from the Indian proto-Tethyan margin to the Australian proto-Tethyan margin.

7. Conclusions

Our new U–Pb zircon ages and whole-rock geochemistry presented in this study support the following conclusions:

- (1) Mafic intrusive rocks from the Pangin area of the Siang window, Eastern Himalaya, north-east India are gabbroic in composition with a sub-alkaline tholeiitic affinity. Their geochemical signatures are similar to E-MORB,

and the parental magma might have been generated by medium to high degrees of partial melting (~12–28%) of an enriched mantle spinel+garnet peridotite source.

- (2) The investigated two gabbro samples yield U–Pb zircon ages of 568 ± 2 Ma and 521.5 ± 2.5 Ma, respectively, indicating Late Neoproterozoic and Early Cambrian magmatic activities in the Siang window.
- (3) These mafic intrusive rocks are geochemically distinct from the earlier reported mafic and felsic volcanics of the Siang window; rather, they may be derived from the melts generated in an extensional tectonic setting.
- (4) Thus, our new geochemical and geochronological data suggest that the studied mafic intrusive rocks of the Siang window were generated during the Late Neoproterozoic to Early Cambrian extensional tectonic environment, similar to those reported from Northwest Himalaya due to the long-lasting Pan-African orogenic cycle which ended with the assembly of the Gondwana supercontinent.

Acknowledgements

The authors are grateful to the Director, Wadia Institute of Himalayan Geology (WIHG), Dehradun for encouragement and permission to publish the present manuscript. We are also thankful to the Lab-in-Charges of XRF, ICPMS, SEM and LA-MC-ICPMS facilities, WIHG for analytical support. Special thanks to Saurabh Singhal, WIHG, for helping with LA-MC-ICPMS U–Pb isotopic analyses. The manuscript has benefited with insightful suggestions from S. Khogenkumar, NCPOR, Goa. This work is part of the ongoing Ph.D. thesis of the first author at BHU, Varanasi and WIHG, Dehradun. We thank Editors-in-Chief, Emeritus Professor Ghislain de Marsily and Professor François Chabaux for their constructive comments. Professor Michel Faure and an anonymous reviewer are thanked for their fruitful suggestions and thorough reviews which helped to improve this study.

References

- Abdel-Rahman, A. F. M. and Nassar, P. E. (2004). Cenozoic volcanism in the Middle East: petrogenesis of alkali basalts from northern Lebanon. *Geol. Mag.*, 141:545–563.
- Acharyya, S. K. (1994). The Cenozoic foreland basin and tectonics of the eastern Sub-Himalaya: problem and prospects. *Himalayan Geol.*, 15:3–21.
- Acharyya, S. K. (1998). Thrust tectonics and evolution of domes and the syntaxis in Eastern Himalaya, India. *J. Nepal Geol. Soc.*, 18:1–17.
- Acharyya, S. K. (2007). Evolution of the Himalayan Paleogene foreland basin, influence of its lithopacket on the formation of thrust-related domes and windows in the Eastern Himalayas - a review. *J. Asian Earth Sci.*, 31:1–17.
- Acharyya, S. K. and Sengupta, S. (1998). The structure of the Siang window, its evolution and bearing on the nature of Eastern syntaxis of the Himalaya. *Natl. Acad. Sci. Lett.*, 21:177–192.
- Ahmad, T. (2008). Precambrian mafic magmatism in the Himalayan mountain range. *J. Geol. Soc. India*, 72(1):85–92.
- Ahmad, T. and Bhat, M. I. (1987). Geochemistry and petrogenesis of the Mandi Darla volcanics, north-western Himalayas. *Precambrian Res.*, 37(3):231–256.
- Ahmad, T., Mukherjee, P. K., and Trivedi, J. R. (1999). Geochemistry of Precambrian mafic magmatic rocks of the western Himalaya, India: petrogenetic and tectonic implications. *Chem. Geol.*, 160(1–2):103–119.
- Ahmad, T. and Tarney, J. (1991). Geochemistry and petrogenesis of Garhwal volcanics: implications for evolution of the north Indian lithosphere. *Precambrian Res.*, 50(1–2):69–88.
- Aldanmaz, E., Pearce, J. A., Thirlwall, M. F., and Mitchell, J. G. (2000). Petrogenetic evolution of late Cenozoic, post-collision volcanism in western Anatolia, Turkey. *J. Volcanol. Geotherm. Res.*, 102:67–95.
- Ali, J. R., Aitchison, J. C., Chik, S. Y. S., Baxter, A. T., and Bryan, S. E. (2012). Paleomagnetic data support Early Permian age for the Abor Volcanics in the lower Siang Valley, NE India: significance for Gondwana-related break-up models. *J. Asian Earth Sci.*, 50:105–115.
- Baig, M. S., Lawrence, R. D., and Snee, L. W. (1988). Evidence for late Precambrian to early Cambrian orogeny in northwest Himalaya, Pakistan. *Geol. Mag.*, 125(1):83–86.
- Bhat, M. I. (1984). Abor volcanics: further evidence

- for the birth of the Tethys Ocean in the Himalayan segment. *J. Geol. Soc. Lond.*, 141:763–775.
- Bhat, M. I. (1987). Spasmodic rift reactivation and its role in the pre-orogenic evolution of the Himalayan region. *Tectonophysics*, 134:103–127.
- Bhat, M. I. and Ahmad, T. (1990). Petrogenesis and the mantle source characteristics of the Abor volcanic rocks, eastern Himalayas. *J. Geol. Soc. India*, 36:227–246.
- Brookfield, M. E. (1993). The Himalayan passive margin from Precambrian to Cretaceous times. *Sedimentary Geol.*, 84(1–4):1–35.
- Buslov, M. M., Safonova, I. Y., Fedoseev, G. S., Reichow, M., Davies, C., and Babin, G. A. (2010). Permo-Triassic plume magmatism of the Kuznetsk Basin, Central Asia: geology, geochronology and geochemistry. *Russ. Geol. Geophys.*, 51:901–916.
- Cawood, P. A. and Buchan, C. (2007). Linking accretionary orogenesis with supercontinent assembly. *Earth-Sci. Rev.*, 82(3–4):217–256.
- Cawood, P. A., Johnson, M. R., and Nemchin, A. A. (2007). Early Palaeozoic orogenesis along the Indian margin of Gondwana: Tectonic response to Gondwana assembly. *Earth Planet. Sci. Lett.*, 255(1–2):70–84.
- Collins, A. S. and Pisarevsky, S. A. (2005). Amalgamating eastern Gondwana: the evolution of the Circum-Indian Orogens. *Earth-Sci. Rev.*, 71(3–4):229–270.
- Cox, K. G., Bell, J. D., and Pankhurst, J. (1979). *The Interpretation of Igneous Rocks*. Allen and Unwin, London.
- Dalziel, I. W. D., Dalla Salda, L. H., and Gahagan, L. M. (1994). Paleozoic Laurentia–Gondwana interaction and the origin of the Appalachian–Andean mountain system. *Geol. Soc. Am. Bull.*, 106:243–252.
- Debon, F., Le Fort, P., Sheppard, S. M. F., and Sonet, J. (1986). The four plutonic belts of the Trans Himalaya: a chemical, mineralogical, isotopic, and chronological synthesis along a Tibet–Nepal granite section. *J. Petrol.*, 21:219–250.
- DePaolo, D. J. (1981). Trace element and isotopic effects of combined wall-rock assimilation and fractional crystallization. *Earth Planet. Sci. Lett.*, 53:189–202.
- Frey, F. A., Weis, D., Borisova, A. Y., and Xu, G. (2002). Involvement of continental crust in the formation of the Cretaceous Kerguelen Plateau: new perspectives from ODP Leg 120 sites. *J. Petrol.*, 43:1207–1239.
- Gaetani, M. and Garzanti, E. (1991). Multicyclic history of the Northern India continental margin (Northwestern Himalaya)(1). *AAPG Bull.*, 75(9):1427–1446.
- Gehrels, G. E., De Celles, P. G., Ojha, T. P., and Upreti, B. N. (2006). Geologic and U–Th–Pb geochronologic evidence for early Paleozoic tectonism in the Kathmandu thrust sheet, central Nepal Himalaya. *Geol. Soc. Am. Bull.*, 118(1–2):185–198.
- Girard, M. and Bussy, F. (1999). Late Pan-African magmatism in the Himalaya: new geochronological and geochemical data from the Ordovician Tso Moriri metagranites (Ladakh, NW India). *Schweiz. Mineralogische und Petrographische Mitteilungen*, 79:399–418.
- Gürsu, S. and Göncüoğlu, M. C. (2005). Early Cambrian back-arc volcanism in the western Taurides, Turkey: implications for rifting along the northern Gondwanan margin. *Geol. Mag.*, 142(5):617–631.
- Gürsu, S., Moeller, A., Göncüoğlu, M. C., Köksal, S., Demircan, H., Köksal, F. T., Kozlu, H., and Sunal, G. (2015). Neoproterozoic continental arc volcanism at the northern edge of the Arabian Plate, SE Turkey. *Precambrian Res.*, 258:208–233.
- Hassanzadeh, J., Stockli, D. F., Horton, B. K., Axen, G. J., Stockli, L. D., Grove, M., Schmitt, A. K., and Walker, J. D. (2008). U–Pb zircon geochronology of late Neoproterozoic–Early Cambrian granitoids in Iran: implications for paleogeography, magmatism, and exhumation history of Iranian basement. *Tectonophysics*, 451(1–4):71–96.
- He, Q., Xiao, L., Balta, B., Gao, R., and Chen, J. (2010). Variety and complexity of the Late-Permian Emeishan basalts: reappraisal of plume–lithosphere interaction process. *Lithos*, 119:91–107.
- Hodges, K. V., Geissman, J. W., and Glazner, A. F. E. (2000). Tectonics of the Himalaya and southern Tibet from two perspectives, Special focus on the Himalaya. *Geol. Soc. Am. Bull.*, 112:324–350.
- Horton, B. K., Hassanzadeh, J., Stockli, D. F., Axen, G. J., Gillis, R. J., Guest, B., Amini, A., Fakhari, M. D., Zamanzadeh, S. M., and Grove, M. (2008). Detrital zircon provenance of Neoproterozoic to Cenozoic deposits in Iran: implications for chronostratigraphy and collisional tectonics. *Tectonophysics*, 451(1–4):97–122.
- Hoskin, P. W. O. and Black, L. P. (2000). Metamorphic

- zircon formation by solid-state recrystallization of protolith igneous zircon. *J. Meteorol. Geol.*, 18:423–439.
- Hughes, N. C. and Jell, P. A. (1999). Biostratigraphy and biogeography of Himalayan Cambrian trilobites. In Macfarlane, A., Sorkhabin, R. B., and Quade, J., editors, *Himalaya and Tibet-Mountain Roots to Mountain Tops*, Special Paper 328, pages 109–116. Geological Society of America.
- Irvine, T. N. J. and Baragar, W. R. A. (1971). A guide to the chemical classification of the common volcanic rocks. *Can. J. Earth Sci.*, 8(5):523–548.
- Islam, R., Upadhyay, R., Ahmad, T., Thakur, V. C., and Sinha, A. K. (1999). Pan-African magmatism and sedimentation in the NW Himalaya. *Gondwana Res.*, 2(2):263–270.
- Jain, A. K. and Thakur, V. C. (1978). Abor volcanics of the Arunachal Himalaya. *J. Geol. Soc. India*, 19:335–349.
- Jain, A. K. and Tondon, S. K. (1974). Stratigraphy and structure of the Siang district, Arunachal (NEFA), Himalaya. *Himalayan Geol.*, 4:28–60.
- Khanna, P. P., Saini, N. K., Mukherjee, P. K., and Purohit, K. K. (2009). An appraisal of ICP-MS technique for determination of REEs: long term QC assessment of silicate Rock Analysis. *Himalayan Geol.*, 30(1):95–99.
- Kumar, G. (1997). *Geology of Arunachal Pradesh*. Geol. Soc. India, Bangalore.
- Kürkcüoğlu, B. (2010). Geochemistry and petrogenesis of basaltic rocks from the Develidag volcanic complex, Central Anatolia, Turkey. *J. Asian Earth Sci.*, 37:42–51.
- Lai, S., Qin, J., Li, Y., Li, S., and Santosh, M. (2012). Permian high Ti/Y basalts from the eastern part of the Emeishan Large Igneous Province, southwestern China: petrogenesis and tectonic implications. *J. Asian Earth Sci.*, 47:216–230.
- Lassiter, J. C. and DePaolo, D. J. (1997). Plume/lithosphere interaction in the generation of continental and oceanic flood basalts: chemical and isotopic constraints. In Mahoney, J. J. and Coffin, M. F., editors, *Large Igneous Province: Continental, Oceanic, and Planetary Flood Volcanism*, Geophysical Monography Series 100, pages 335–355. American Geophysical Union.
- Lassiter, J. C., DePaolo, D. J., and Mahoney, J. J. (1995). Geochemistry of the Wrangellia Flood Basalt Province: implications for the role of continental and oceanic lithosphere in Flood Basalt Genesis. *J. Petrol.*, 36:983–1009.
- Le Fort, P., Debon, F., Pecher, A., Sonet, J., and Vidal, P. (1986). The 500 Ma magmatic event in Alpine southern Asia, a thermal episode at Gondwana Scale. *Sci. Terre, Mem.*, 47:191–209.
- Le Fort, P., Tongiorgi, M., and Gaetani, M. (1994). Discovery of a crystalline basement and early Ordovician marine transgression in the Karakoram mountain range, Pakistan. *Geology*, 22:941–944.
- Li, X. H., Li, W. X., Li, Z. X., and Liu, Y. (2008a). 850–790 Ma bimodal volcanic and intrusive rocks in northern Zhejiang, South China: a major episode of continental rift magmatism during the breakup of Rodinia. *Lithos*, 102:341–357.
- Li, Z. X., Bogdanova, S. V., Collins, A. S., Davidson, A., De Waele, B., Ernst, R. E., Fitzsimons, I. C. W., Fuck, R. A., Gladkochub, D. P., Jacobs, J., and Karlstrom, K. E. (2008b). Assembly, configuration, and breakup history of Rodinia: a synthesis. *Precambrian Res.*, 160(1–2):179–210.
- Liebke, U., Antolin, B., Appel, E., Basavaiah, N., Mikes, T., Dunkl, I., and Wemmer, K. (2011). Indication for Clockwise Rotation in the Siang Window South of the eastern Himalayan Syntaxis and new Geochronological Constraints for the Area. *Geol. Soc. Lond. (Special Publications)*, 353:71–97.
- Liu, C., Zhao, G., Liu, F., Sun, M., Zhang, J., and Yin, C. (2012). Zircons U–Pb and Lu–Hf isotopic and whole-rock geochemical constraints on the Gantaohu Group in the Zhanhuang Complex: implications for the tectonic evolution of the Trans-North China Orogen. *Lithos*, 146:80–92.
- Mahmoud, R. I., Wali, F. S., František, H. V., Jan, K., and Wolfgang, F. (2011). Magmatic and metamorphic evolution of the ShoturKuh metamorphic complex (Central Iran). *Int. J. Earth Sci.*, 100:45–62.
- Manikyamba, C., Kerrich, R., Naqvi, S. M., and Rammohan, M. (2004). Geochemical systematics of tholeiitic basalts from the 2.7 Ga Ramgiri-Hungund greenstone belt, Dharwarcraton: an intraoceanic arc. *Precambrian Res.*, 134:21–39.
- McKenzie, D. and O’Nions, P. K. (1991). Partial melt distribution from inverse of rare earth element concentrations. *J. Petrol.*, 32:1021–1091.
- Meert, J. G. (2003). A synopsis of events related to the assembly of eastern Gondwana. *Tectonophysics*, 362:1–40.
- Meert, J. G. and Lieberman, B. S. (2008). The Neopro-

- terozoic assembly of Gondwana and its relationship to the Ediacaran–Cambrian radiation. *Gondwana Res.*, 14:5–21.
- Meert, J. G. and Van Der Voo, R. (1997). The assembly of Gondwana 800–550 Ma. *J. Geodyn.*, 23(3–4):223–235.
- Menzies, M. A., Kyle, P. R., Jones, M., and Ingram, G. (1991). Enriched and depleted source components for tholeiitic and alkaline lavas from Zuni-Bandera, New Mexico: inferences about intraplate processes and stratified lithosphere. *J. Geophys. Res.*, 96:13645–13671.
- Miller, C., Thöni, M., Frank, W., Grasemann, B., Klötzli, U., Guntli, P., and Draganits, E. (2001). The Early Palaeozoic magmatic event in the Northwest Himalaya, India: source, tectonic setting and age of emplacement. *Geol. Mag.*, 138(3):237–251.
- Mukherjee, P. K., Singhal, S., Adlakha, V., Rai, S. K., Dutt, S., Kharya, A., and Gupta, A. K. (2017). In situ U–Pb zircon micro-geochronology of MCT zone rocks in the Lesser Himalaya using LA-MC-ICPMS technique. *Curr. Sci.*, 112:802–810.
- Murphy, J. B. and Nance, R. D. (1991). Supercontinent model for the contrasting character of Late Proterozoic orogenic belts. *Geology*, 19:469–472.
- Murphy, J. B., van Staal, C. R., and Collins, W. J. (2011). A comparison of the evolution of arc complexes in Paleozoic interior and peripheral orogens: speculations on geodynamic correlations. *Gondwana Res.*, 19(3):812–827.
- Nadimi, A. (2007). Evolution of the Central Iranian basement. *Gondwana Res.*, 12(3):324–333.
- Paton, C., Hellstrom, J., Paul, B., Woodhead, J., and Hergt, J. (2011). Iolite: freeware for the visualisation and processing of mass spectrometric data. *J. Anal. At. Spectrom.*, 26(12):2508–2518.
- Pearce, J. A. (2008). Geochemical fingerprinting of oceanic basalts with applications to ophiolite classification and the search for Archaean oceanic crust. *Lithos*, 100:14–48.
- Pearce, J. A. (2014). Immobile element fingerprinting of ophiolites. *Elements*, 10:101–108.
- Pearce, J. A., Alabaster, T., Shelton, A. W., and Searle, M. P. (1981). The Oman ophiolite as a Cretaceous arc-basin complex: evidence and implications. *Phil. Trans. R. Soc. Lond. A*, 300(1454):299–317.
- Pearce, J. A. and Cann, J. (1973). Tectonic setting of basic volcanic rocks determined using trace element analyses. *Earth Planet. Sci. Lett.*, 19:290–300.
- Pearce, J. A. and Norry, M. J. (1979). Petrogenetic implications of Ti, Zr, Y and Nb variations in volcanic rocks. *Cont. Mineral. Petrol.*, 69:33–47.
- Pearce, J. A. and Peate, D. W. (1995). Tectonic implications of the composition of volcanic arc magmas. *Annu. Rev. Earth Planet. Sci. Lett.*, 23:251–285.
- Pearce, J. A., Sieger, R., Arculus, R. C., Murton, B. J., Ishii, T., Peate, D. W., and Parkinson, I. J. (1992). Boninite and Harzburgite from Leg 125 (Bonin-Mariana Forearc): a case study of magma genesis during the initial stages of subduction. *Proc. Ocean Drill. Program Sci. Results*, 125:623–659.
- Polat, A., Hofmann, A. W., and Rosing, M. (2002). Boninite-like volcanic rocks in the 3.7–3.8 Ga Suisa greenstone belt, West Greenland: geochemical evidence for intra-oceanic subduction zone processes in the early Earth. *Chem. Geol.*, 184:231–254.
- Ramezani, J. and Tucker, R. D. (2003). The Saghand region, central Iran: U–Pb geochronology, petrogenesis and implications for Gondwana tectonics. *Am. J. Sci.*, 303(7):622–665.
- Regelous, M., Hofmann, A. W., Abouchami, W., and Galer, S. J. G. (2003). Geochemistry of lavas from the Emperor seamounts, and the geochemical evolution of Hawaiian magmatism from 85 to 42 Ma. *J. Petrol.*, 44:113–140.
- Reichow, M. K., Saunders, A. D., White, R. V., Al'Mukhamedov, A. I., and Medvedev, A. Y. (2005). Geochemistry and petrogenesis of basalts from the West Siberian Basin: an extension of the Permo-Triassic Siberian Traps, Russia. *Lithos*, 79:425–452.
- Rollinson, H. R. (1993). *Using Geochemical Data: Evaluation, Presentation, Interpretation*. John Wiley, Chichester. 352 p.
- Rudnick, R. L. and Gao, S. (2003). The composition of the continental crust. In Rudnick, R. L., Holland, H. D., and Turekian, K. K., editors, *The Crust Treatise on Geochemistry*, 3, pages 1–64. Elsevier, Oxford.
- Saccani, E. (2015). A new method of discriminating different types of post-Archaean ophiolitic basalts and their tectonic significance using Th–Nb and Ce–Dy–Yb systematics. *Geosci. Front.*, 6:481–501.
- Safonova, I. Y., Simonov, V. A., Buslov, M. M., Ota, T., and Maruyama, S. (2008). Neoproterozoic basalts of the Paleo-Asian Ocean (Kurai accretion zone, Gorny Altai, Russia): geochemistry, petrogenesis, geodynamics. *Russ. Geol. Geophys.*, 49:254–271.

- Saini, N. K., Khanna, P. P., Mukherjee, P. K., and Rathi, M. S. (2003). Determination of Major and Trace elements in Silicate reference samples using XRF and ICP-AES techniques: a comparative study. *Himalayan Geol.*, 24(2):117–119.
- Saki, A. (2010). Proto-Tethyan remnants in northwest Iran: geochemistry of the gneisses and metapelitic rocks. *Gondwana Res.*, 17(4):704–714.
- Sengör, A. M. C. and Natal'in, B. A. (1996). Paleotectonics of Asia: fragments of a synthesis. In Yin, A. and Harrison, T. M., editors, *The Tectonic Evolution of Asia*, pages 486–640. Cambridge University Press, Cambridge.
- Sengupta, S., Acharyya, S. K., and DeSmeth, J. B. (1996). Geochemical characteristics of the Abor volcanic rocks, NE Himalaya, India: nature and early Eocene magmatism. *J. Geol. Soc. Lond.*, 153:695–704.
- Shervais, J. W. (1982). Ti-V plots and the petrogenesis of modern and ophiolitic lavas. *Earth Planet. Sci. Lett.*, 59(1):101–118.
- Singh, A. K. (2006). Petrography, geochemistry and petrogenesis of Abor Volcanics, eastern Himalayan Syntaxial bend. *Himalayan Geol.*, 27:163–181.
- Singh, A. K. (2007). Chemical characteristics of alkaline basalt from the Abor Volcanics of Arunachal Himalaya. *J. Geol. Soc. India*, 69:1189–1194.
- Singh, A. K. (2012). Geochemical Constraints on the Petrogenesis and Tectonic Environment of Gabbroic Intrusives in the Siang Window of Eastern Himalaya, Northeast India. *J. Geol. Soc. India*, 79:576–588.
- Singh, A. K., Chung, S. L., Bikramaditya Singh, R. K., Lee, H.-Y., and Khogenkumar, S. (2019). Zircon U–Pb geochronology, Hf isotopic compositions, and petrogenetic study of Abor volcanic rocks of Eastern Himalayan Syntaxis, Northeast India: implications for eruption during breakup of eastern Gondwana. *Geol. J.*, 55(2):1227–1244.
- Singh, A. K. and Singh, R. K. B. (2012). Petrogenetic evolution of the felsic and mafic volcanic suite in the Siang Window of eastern Himalaya, Northeast India. *Geosci. Front.*, 3(5):613–634.
- Singh, A. K. and Tewari, V. C. (2010). Geochemical and biostratigraphic constraints on the genesis of mafic intrusive in the Buxa Dolomite (Neoproterozoic), Panging area of the Arunachal Lesser Himalaya, Northeast India. *J. Nepal Geol. Soc.*, 40:1–12.
- Singh, S. (1993). Geology and tectonics of the eastern syntaxial bend, Arunachal Himalaya. *Himalayan Geol.*, 4:149–163.
- Singh, T. (1999). Palaeontological records from the eastern Himalayas: a synthesis. In Verma, P. K., editor, *Geological Studies in the Eastern Himalayas*, pages 129–163. Pilgrims Book, Delhi.
- Slama, J., Kosler, J., Condon, D. J., Crowley, J. L., Gerdes, A., Hanchar, J. M., Horstwood, M. S. A., Morris, G. A., Nasdala, L., Norberg, N., Schaltegger, U., Schoene, B., Tubrett, M. N., and Whitehouse, M. J. (2008). Plešovice zircon—A new natural reference material for U–Pb and Hf isotopic microanalysis. *Chem. Geol.*, 249:1–35.
- Srivastava, R. K. and Sahai, A. (2001). High-field strength element geochemistry of mafic intrusive rocks from the Bhagirathi and Yamuna valleys, Garhwal Himalaya, India. *Gondwana Res.*, 4(3):455–463.
- Stacey, J. C. and Kramers, J. D. (1975). Approximation of terrestrial lead isotope evolution by a two-stage model. *Earth Planet. Sci. Lett.*, 26:207–221.
- Staudigel, H., Plank, T., White, B., and Schmincke, H. U. (1996). Geochemical fluxes during seafloor alteration of the basaltic upper oceanic crust: DSDP sites 417 and 418. In Bebout, G. E., Scholl, S. W., Kirby, S. H., and Platt, J. P., editors, *Subduction Top to Bottom*, pages 19–38. American Geophysical Union, Washington, D.C.
- Stern, R. J. (1994). Arc assembly and continental collision in the Neoproterozoic East African Orogen: implications for the consolidation of Gondwana. *Annu. Rev. Earth Planet. Sci.*, 22:319–351.
- Sun, S. S. and McDonough, W. F. (1989). Chemical and isotopic systematics of oceanic basalts: implications for mantle composition and processes. In Saunders, A. D. and Norry, M. J., editors, *Magma-tism in Ocean Basins*, Geol. Soc. London Spec. Pub. 42, pages 313–345.
- Talukdar, S. C. and Majumdar, A. K. (1983). Geology of the Abor volcanic rocks, Siang district, Arunachal Pradesh. In *Proc. Symp. Geol. Miner. Resour. NE Himalayas*, Geol. Surv. India, Misc. Pub. 43, pages 135–138.
- Taylor, S. R. and McLennan, S. M. (1985). *The Continental Crust: Its Composition and Evolution*. Oxford Blackwell Scientific Publications, London. 312 p.
- Ustaömer, P. A., Ustaömer, T., Collins, A. S., and

- Robertson, A. H. (2009). Cadomian (Ediacaran–Cambrian) arc magmatism in the Bitlis Massif, SE Turkey: magmatism along the developing northern margin of Gondwana. *Tectonophysics*, 473(1–2):99–112.
- Valdiya, K. S. (1995). Proterozoic sedimentation and Pan-African geodynamic development in the Himalaya. *Precambrian Res.*, 74:35–55.
- Vermeesch, P. (2018). Isoplot R: a free and open toolbox for geochronology. *Geosci. Front.*, 9:1479–1493.
- Wadia, D. N. (1931). The syntaxis of Northwest Himalaya: its rocks, tectonics and orogeny. *Rec. Geol. Surv. India*, 6:189–220.
- Weyer, S., Münker, C., and Mezger, K. (2003). Nb/Ta, Zr/Hf and REE in the depleted mantle: implications for the differentiation history of the crust–mantle system. *Earth Planet. Sci. Lett.*, 205(3):309–324.
- White, R. S. and McKenzie, D. (1995). Mantle plumes and flood basalts. *J. Geophys. Res.*, 100:17543–17585.
- Wiedenbeck, M., Alle, P., Corfu, F., Griffin, W. L., Meier, M., Oberli, F., von Quadt, A., Roddick, J. C., and Spiegel, W. (1995). Three natural zircon standards for U–Th–Pb, Lu–Hf, trace element and REE analyses. *Geostandards Newsl.*, 19:1–23.
- Winchester, J. A. and Floyd, P. A. (1977). Geochemical discrimination of different magma series and their differentiation products using immobile elements. *Chem. Geol.*, 20:325–345.
- Xu, Y.-G., Ma, J. L., Frey, F. A., Feigenson, M. D., and Liu, J.-F. (2005). Role of lithosphere asthenosphere interaction in the genesis of Quaternary alkali and tholeiitic basalts from Datong, western North China Craton. *Chem. Geol.*, 224(4):247–271.
- Yaxley, G. M. (2000). Experimental study of the phase and melting relations of homogeneous basalt + peridotite mixtures and implications for the petrogenesis of flood basalts. *Cont. Mineral. Petrol.*, 139:326–338.
- Yin, A. (2006). Cenozoic tectonic evolution of the Himalayan orogen as constraint by along-strike variation of structural geometry, exhumation history, and foreland sedimentation. *Earth Sci. Rev.*, 76:1–131.
- Zhao, J. H. and Zhou, M. F. (2007). Geochemistry of Neoproterozoic mafic intrusions in the Panzhihua district (Sichuan Province, SW China): implications for subduction related metasomatism in the upper mantle. *Precambrian Res.*, 152:27–47.
- Zhu, D. C., Zhao, Z. D., Niu, Y., Dilek, Y., Wang, Q., Ji, W. H., Dong, G. C., Sui, Q. L., Liu, Y. S., Yuan, H. L., and Mo, X. X. (2012). Cambrian bimodal volcanism in the Lhasa Terrane, southern Tibet: record of an early Paleozoic Andean-type magmatic arc in the Australian proto-Tethyan margin. *Chem. Geol.*, 328:290–308.